

Cite this: *Nanoscale Adv.*, 2021, 3, 3708

# Recent advances in graphite carbon nitride-based nanocomposites: structure, antibacterial properties and synergies

Kai Yan,<sup>ab</sup> Chenglong Mu,<sup>b</sup> Lingjie Meng,<sup>id</sup>\*<sup>ac</sup> Zhaofu Fei<sup>id</sup>\*<sup>d</sup> and Paul J. Dyson<sup>id</sup>\*<sup>d</sup>

Bacterial infections and transmission threaten human health and well-being. Graphite carbon nitride (g-C<sub>3</sub>N<sub>4</sub>), a promising photocatalytic antibacterial nanomaterial, has attracted increasing attention to combat bacterial transmission, due to the outstanding stability, high efficiency and environmental sustainability of this material. However, the antibacterial efficiency of g-C<sub>3</sub>N<sub>4</sub> is affected by several factors, including its specific surface area, rapid electron/hole recombination processes and optical absorption properties. To improve the efficiency of the antibacterial properties of g-C<sub>3</sub>N<sub>4</sub> and extend its range of applications, various nanocomposites have been prepared and evaluated. In this review, the advances in amplifying the photocatalytic antibacterial efficiency of g-C<sub>3</sub>N<sub>4</sub>-based nanocomposites is discussed, including different topologies, noble metal decoration, non-noble metal doping and heterojunction construction. The enhancement mechanisms and synergistic effects in g-C<sub>3</sub>N<sub>4</sub>-based nanocomposites are highlighted. The remaining challenges and future perspectives of antibacterial g-C<sub>3</sub>N<sub>4</sub>-based nanocomposites are also discussed.

Received 5th April 2021  
Accepted 27th May 2021DOI: 10.1039/d1na00257k  
rsc.li/nanoscale-advances

## 1. Introduction

Bacterial infections and their transmission pose a considerable threat to human health, usually leading to delayed wound healing and chronic intestinal diseases.<sup>1,2</sup> Furthermore, pathogenic bacteria frequently contaminate water supplies and the soil, resulting in the death of animals and plants through environmental contamination.<sup>3</sup> To address these problems, antibiotics are widely used to kill bacteria, but over-utilization of antibiotics can bring about resistance and secondary contamination.<sup>4-6</sup> Therefore, the development of new strategies

<sup>a</sup>School of Chemistry, MOE Key Laboratory for Nonequilibrium Synthesis and Modulation of Condensed Matter, Xi'an Key Laboratory of Sustainable Energy Material Chemistry, Xi'an Jiaotong University, Xi'an 710049, P. R. China. E-mail: menglingjie@mail.xjtu.edu.cn

<sup>b</sup>College of Bioresources Chemical and Materials Engineering, Shaanxi University of Science and Technology, Xi'an 710021, China

<sup>c</sup>Instrumental Analysis Center, Xi'an Jiaotong University, Xi'an 710049, P. R. China

<sup>d</sup>Institut des Sciences et Ingénierie Chimiques, Ecole Polytechnique Fédérale de Lausanne (EPFL), CH-1015 Lausanne, Switzerland. E-mail: zhaofu.feifei@epfl.ch; pjd@epfl.ch



Kai Yan is a lecturer at the College of Bioresources Chemical and Materials Engineering in Shaanxi University of Science and Technology. He received his PhD degree from Fudan University in 2017. His current research interest is mainly focused on multifunctional nanomaterials for biological applications.



Lingjie Meng is a professor at the School of Chemistry in Xi'an Jiaotong University. He received his PhD degree from Xi'an Jiaotong University in 2005 and was a lecturer in Shanghai Jiaotong University from 2005 to 2010. He became an associate professor in 2011. He was a visiting scholar at the University of Texas at Austin from 2011 to 2012. In 2013, he was appointed as a Professor in

Xi'an Jiaotong University. His research interests are focused on the nanomaterials for theranostics.



to inactivate bacteria without using antibiotics is urgently required as is the inactivation of drug-resistant bacteria. In recent years, semiconductor photocatalysis has attracted significant interest for applications in pollutant degradation<sup>7</sup> and antimicrobial applications.<sup>8</sup> Under sunlight irradiation, semiconductor photocatalysts react with water and oxygen to form reactive oxygen species (ROS), such as hydrogen peroxide ( $\text{H}_2\text{O}_2$ ), hydroxyl radicals ( $\cdot\text{OH}$ ) and superoxide ( $\text{O}_2^{\cdot-}$ ), which are able to inactivate bacteria by oxidizing the phospholipid membrane, proteins and nucleic acids.<sup>9–13</sup> Common photocatalysts include metallic oxides, sulfides, nitrides, and phosphides, and graphene and its derivatives,<sup>14,15</sup> which show bactericidal activity against both Gram-positive and Gram-negative bacteria, as demonstrated in many studies. However, relatively narrow spectral absorption ranges result in low efficiencies.<sup>16</sup> Together with other problems such as facile aggregation, potential toxicity, and low biocompatibility, practical application of these common photocatalysts is limited. As an emerging non-metallic photocatalyst, graphitic carbon nitride ( $\text{g-C}_3\text{N}_4$ ) is easy to prepare and has an appropriate band structure and good biocompatibility,<sup>17</sup> thus showing considerable potential as antibacterial materials.

Similar to the layered structure of graphene,  $\text{g-C}_3\text{N}_4$  is a polymeric layered material which consists of carbon and nitrogen with some hydrogen (impurity). The conduction band (CB) and valence band (VB) position of  $\text{g-C}_3\text{N}_4$  are  $\sim 1.13$  and  $1.57$  eV, respectively. The appropriate band gap is about  $2.70$  eV, *i.e.* it is a medium band gap semiconductor, readily obtained from the pyrolysis of melamine, dicyandiamide or urea. Benefiting from the connection of tri-*s*-triazine units through tertiary amines (Fig. 1),  $\text{g-C}_3\text{N}_4$  has a two-dimensional flake structure. The adjacent  $\text{g-C}_3\text{N}_4$  flakes interact weakly with each other *via* van der Waals forces, displaying a layer gap of about  $0.33$  nm.<sup>18–22</sup> Thus, when such forces between the bulk  $\text{g-C}_3\text{N}_4$  layers are broken, paper-like  $\text{g-C}_3\text{N}_4$  nanosheets are obtained.<sup>23–27</sup> From a molecular prospective,  $\text{C}_3\text{N}_4$  is considered to have two main molecular structures. One comprises a triazine with a tertiary nitrogen atom in the center of a planar triangle (Fig. 1a) that connects three separate triazine rings in an infinitely repeating pattern.<sup>28</sup> Another is a tri-*s*-triazine structurally

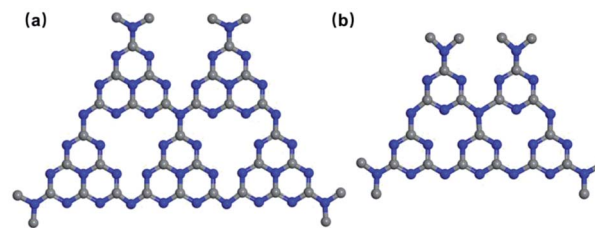


Fig. 1 (a) Tri-*s*-triazine and (b) *s*-triazine structure of  $\text{g-C}_3\text{N}_4$ .

connected to form  $\text{g-C}_3\text{N}_4$  (Fig. 1b). This more stable tri-*s*-triazine structure is commonly used as the structural unit of  $\text{g-C}_3\text{N}_4$ .<sup>29</sup> These excellent structural features and properties make  $\text{C}_3\text{N}_4$  a promising photocatalytic material. Since the first study of the photocatalytic activity of  $\text{g-C}_3\text{N}_4$  by Wang *et al.* in 2009, it has become a prevalent photocatalytic material.<sup>30</sup> Due to the merits of the non-metallic  $\text{g-C}_3\text{N}_4$  material, such as a wide visible light absorption range, excellent chemical stability and low toxicity, it has been widely studied to tackle environmental and energy related problems.<sup>31–35</sup> Specifically,  $\text{g-C}_3\text{N}_4$  has been used as a catalyst for photocatalytic water reduction and oxidation, contaminant degradation and carbon dioxide reduction.<sup>36–41</sup> For photocatalytic degradation, the photo-produced electrons ( $\text{e}^-$ ) and holes ( $\text{h}^+$ ) can accelerate reduction and oxidation degradation reactions.<sup>42–47</sup> In addition, the  $\text{e}^-$  and  $\text{h}^+$  can react with surrounding  $\text{H}_2\text{O}$  and  $\text{O}_2$  to generate ROS such as  $\cdot\text{O}^2-$  and  $\cdot\text{OH}^-$ . The generated ROS can further degrade pollutants, combining to achieve the removal of contaminants.<sup>48–51</sup>

In this review, several tactics for enhancing the antimicrobial efficiency of  $\text{g-C}_3\text{N}_4$ -based nanocomposites are discussed (Fig. 2), including the design of different  $\text{g-C}_3\text{N}_4$  topologies,<sup>52–55</sup> noble metal decoration,<sup>56–58</sup> non-noble metal doping and heterojunction construction.<sup>59–61</sup> These approaches have been shown to effectively boost the antibacterial activity of  $\text{g-C}_3\text{N}_4$ .<sup>62–67</sup> The enhancement mechanisms and synergistic effects of  $\text{g-C}_3\text{N}_4$ -based nanocomposites is highlighted. Additionally, photocatalytic mechanisms have been elucidated by analyzing the interactions between the nanomaterials and bacteria.



Zhaofu Fei is a senior research scientist in the Institute of Chemical Sciences and Engineering at the Ecole Polytechnique Fédérale de Lausanne (EPFL). He received his PhD degree from the Technical University of Braunschweig, Germany in 1999. After postdocs in the UK and Germany he joined EPFL in 2002. His research interests are focused on design and synthesis of ionic

liquids and related nanomaterials.



Paul J. Dyson is a professor in the Institute of Chemical Sciences and Engineering at the EPFL. He received his PhD degree from the University of Edinburgh in 1993 and subsequently held positions at Imperial College of Science, Technology and Medicine and the University of York. His research interests are focused on synthesis and properties of compounds and materials with

applications in catalysis and medicine.



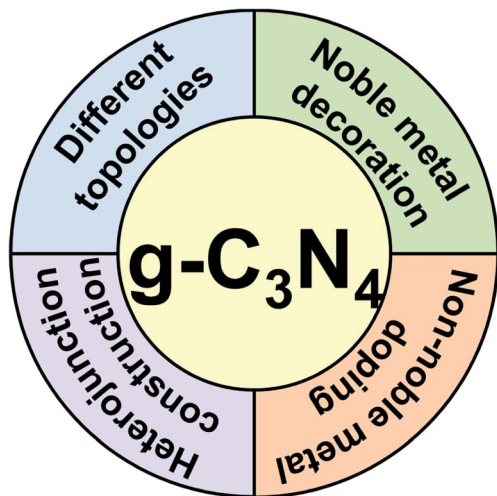


Fig. 2 Schematic illustration of antimicrobial enhancement of  $g\text{-C}_3\text{N}_4$ -nanomaterials.

Lastly, this review concludes by defining future prospects, opportunities and challenges in this exciting field.

## 2. $g\text{-C}_3\text{N}_4$ -based materials and their photocatalytic antibacterial

Both the nitrogen and carbon atoms in  $g\text{-C}_3\text{N}_4$  are  $sp^2$  hybridized to form a conjugated structure with delocalized  $\pi$ -electrons, giving  $g\text{-C}_3\text{N}_4$  the lowest bandgap compared to other phases of  $\text{C}_3\text{N}_4$ .<sup>68</sup> Compared to other conventional photocatalytic materials,  $g\text{-C}_3\text{N}_4$  has a narrow band gap (2.7 eV), resulting in a wider spectral absorption range of up to 460 nm, and improving the photocatalytic window.<sup>69</sup> The photocatalytic reactions of  $g\text{-C}_3\text{N}_4$  affect its antibacterial performance. When the energy of the visible light illuminating  $g\text{-C}_3\text{N}_4$  is larger than the band gap energy of  $g\text{-C}_3\text{N}_4$ ,  $e^-$  are promoted from the valence band (VB) to the conduction band (CB), producing active  $e^-$  and  $h^+$ . However, the  $e^-/h^+$  can recombine on the  $g\text{-C}_3\text{N}_4$  surface. Alternatively, the  $e^-/h^+$  pairs diffuse or are transported to the  $g\text{-C}_3\text{N}_4$  interface by an electric field and undergo redox reactions with the surroundings. As shown in Fig. 3, under visible light illumination,  $g\text{-C}_3\text{N}_4$  produces ROS that can destroy the bacterial membranes, causing cell membrane permeability, structural degradation and ultimately killing the bacterial.<sup>70</sup>



Fig. 3 Plausible reactions between bacterial and  $g\text{-C}_3\text{N}_4$ -based nanocomposite generated ROS.

### 2.1 Influence of topology on $g\text{-C}_3\text{N}_4$ -based antibacterial photocatalysts

The antibacterial activity of  $g\text{-C}_3\text{N}_4$  is influenced by its topology, in particular, the efficiency of bulk  $g\text{-C}_3\text{N}_4$  is restricted by its small superficial area and rapid rate of recombination of photogenerated carriers.<sup>71–75</sup> In contrast, mesoporous  $g\text{-C}_3\text{N}_4$ ,  $g\text{-C}_3\text{N}_4$  nanotubes and nanosheets absorb visible light more effectively and provide a larger contact area for reactants because of their larger specific surface areas and a larger number of active sites.<sup>76,77</sup> In addition, these structures decrease the distance required for the transfer of the charge to the surface of the material, decreasing charge recombination.<sup>78,79</sup> Moreover, due to the quantum size effects,  $g\text{-C}_3\text{N}_4$  nanosheets are suited to charge transfer and separation processes.<sup>80,81</sup> Therefore,  $g\text{-C}_3\text{N}_4$  nanosheets and their composite materials show promising photocatalytic antibacterial properties. Li *et al.* developed a self-cleaning antibacterial membrane by simply filtering  $g\text{-C}_3\text{N}_4$  nanosheets into polyacrylonitrile porous substrates (Fig. 4a), then forming a stable coating by cross-linking polyvinyl alcohol and glutaraldehyde.<sup>82</sup> In contrast to membranes without  $g\text{-C}_3\text{N}_4$  nanosheets, the membranes containing the  $g\text{-C}_3\text{N}_4$  nanosheets (0.45 wt%) completely inactivated  $1 \times 10^6$  cfu  $\text{mL}^{-1}$  *E. coli* under irradiation with visible light (Fig. 4b and c). The high superficial area of the  $g\text{-C}_3\text{N}_4$  nanosheets in the membrane provides more active sites that produce ROS for sterilization. Meanwhile, the membranes with  $g\text{-C}_3\text{N}_4$  nanosheets also showed good permeability to water and degraded dyes. Compared to  $g\text{-C}_3\text{N}_4$  nanosheets, nanotubes have high aspect ratios, a topology that favors the migration of  $e^-$  along the axial direction and inhibits the lateral transfer of  $e^-$ , thereby inhibiting the recombination of photogenerated carriers. Moreover, nanotubes usually have large specific surface areas, providing a higher density of active sites at their surface, which improves photocatalytic antibacterial performance.<sup>83,84</sup> Xu *et al.* successfully synthesized microtubular nanoporous  $g\text{-C}_3\text{N}_4$  with a layered structure and nitrogen defects using molecular self-assembly methods.<sup>85</sup> The hexagonal tubular structure promotes the multiple use of light, and provides a larger density active sites and a directional transfer channel for  $e^-$ . Moreover, the nanoporosity of the material increases the specific surface area to provide rich charge transport paths. In addition, the nitrogen vacancies improve the light harvesting properties of the material ( $\lambda > 450$  nm) and promote charge separation by trapping charge. Hence, microtubular nanoporous  $g\text{-C}_3\text{N}_4$  completely inactivated  $5 \times 10^6$  cfu  $\text{mL}^{-1}$  *E. coli* after 4 h of light illumination, compared to only 74% of *E. coli* sterilized by bulk  $g\text{-C}_3\text{N}_4$ . Hollow porous microspheres not only promote light penetration within the material and light absorption at the pore edges, but also provide sufficient contact area to accelerate interfacial charge transfer. In addition, the thinner pore wall structure reduces the distance (and time) required for charge transfer within the material, decreasing the recombination of photogenerated carriers.<sup>86</sup> Yang *et al.* successfully fabricated a self-cleaning, antimicrobial and antifouling membrane by integrating mesoporous  $g\text{-C}_3\text{N}_4$  (MCN) into polyvinylidene fluoride





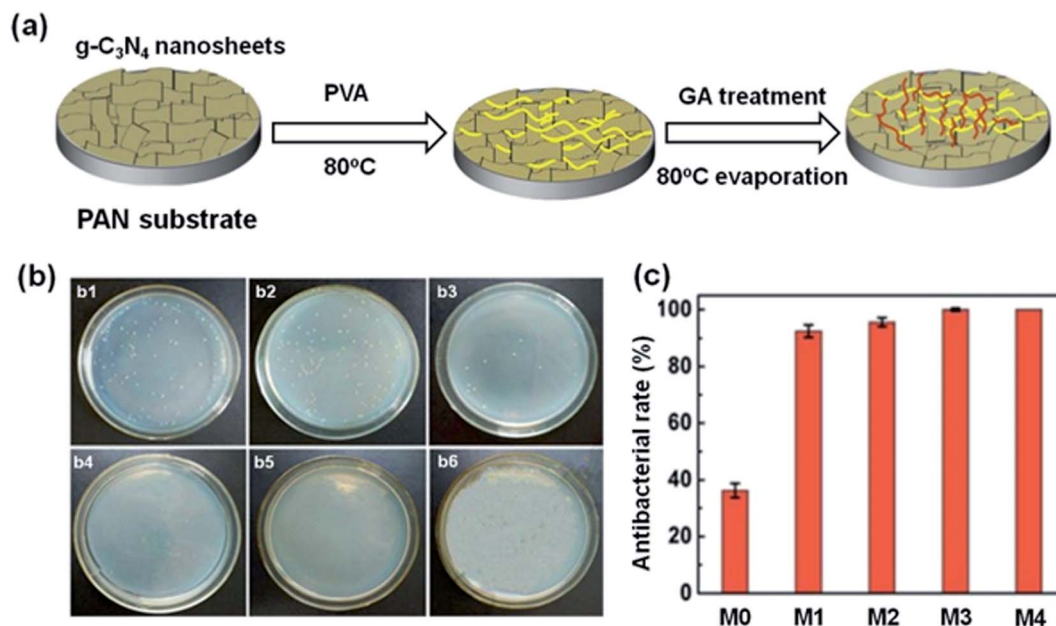


Fig. 4 (a) Preparation of  $g\text{-C}_3\text{N}_4$  nanosheet-functionalized composite membranes. The concentration of  $g\text{-C}_3\text{N}_4$  nanosheets in the membrane are 0, 0.15 wt%, 0.3 wt%, 0.45 wt%, 0.6 wt% in M0, M1, M2, M3, M4, respectively. (b) Antimicrobial activities against *E. coli* of (b1) control, (b2) M0, (b3) M1, (b4) M2, (b5) M3, (b6) M4. (c) Antibacterial rate of membranes M0, M1, M2, M3, M4. Reproduced from ref. 82 with permission from Royal Society of Chemistry, copyright 2017.

(PVDF).<sup>87</sup> The mesoporous structure promotes multiple reflections of incident light and enhances the capacity of the material for light capture, leading to an enhancement in the generation of  $h^+$  and ROS. The MCN-PVDF membrane showed a significant

reduction in the number of *E. coli* colonies under illumination with visible light over 4 hours, with approximately 3 log deactivation of *E. coli*.<sup>88,89</sup> In contrast, an analogous experiment using a membrane-free material showed no significant decrease

Table 1 Antibacterial properties of  $g\text{-C}_3\text{N}_4$  based materials with different topologies

Material	Preparation	Bacteria	Effect	Ref.
$g\text{-C}_3\text{N}_4$ nanosheets	Acid etching and ultrasound	<i>E. coli</i>	~100%	82
Microtubular nanoporous $g\text{-C}_3\text{N}_4$	Molecular self-assembly	<i>E. coli</i>	99.2%	85
$g\text{-C}_3\text{N}_4$ nanosheets	Freezing and microwave-assisted	<i>E. coli</i>	100%	90
Porous $g\text{-C}_3\text{N}_4$ nanosheets	Template-free	<i>E. coli</i>	100%	91
$g\text{-C}_3\text{N}_4$ nanosheets	Bacterial etching	<i>E. coli</i>	3.65 log	92
$g\text{-C}_3\text{N}_4$ nanosheets	Ultrasound	<i>E. coli</i> O157:H7	0.82 log	93
		<i>S. aureus</i>	0.85 log	
$g\text{-C}_3\text{N}_4$ nanosheets	Chemical exfoliation	<i>E. coli</i> K-12	6.5 log	94
$g\text{-C}_3\text{N}_4$ nanosheets	Ultrasound	<i>E. coli</i>	99%	95
bare $g\text{-C}_3\text{N}_4$	Calcination	MS2	100%	96
Mesoporous $g\text{-C}_3\text{N}_4$	Immersion-precipitation phase transformation	<i>E. coli</i>	3 log	87
Mesoporous $g\text{-C}_3\text{N}_4$	Template method	<i>E. coli</i> K-12	99%	97
Mesoporous $g\text{-C}_3\text{N}_4$	Thermal polymerization and selective dialysis approach	<i>E. coli</i>	99%	98
		<i>S. aureus</i>	90%	
$\text{Ag}_2\text{WO}_4$ /mesoporous $g\text{-C}_3\text{N}_4$	Polymerization	<i>E. coli</i>	100%	99
GO quantum dots/oxidized nanoporous $g\text{-C}_3\text{N}_4$	Self-assembly	<i>E. coli</i>	99.6%	100
Nanomesh $g\text{-C}_3\text{N}_4$	Template method	<i>E. coli</i> K-12	85%	101
$\text{CuInSe}_2\text{:Zn/g-C}_3\text{N}_4\text{/TiO}_2$ nanowire	<i>In situ</i> growth	<i>S. aureus</i>	90%	102
Mesoporous $g\text{-C}_3\text{N}_4$	Thermal, polycondensation	<i>E. coli</i>	Effective	103
Porous $g\text{-C}_3\text{N}_4$	Calcination	<i>S. aureus</i>	99%	104
Mesoporous $g\text{-C}_3\text{N}_4$	Calcination	<i>E. coli</i>	Effective	105
Nanostructured $g\text{-C}_3\text{N}_4$	Calcination	<i>E. coli</i> O157:H	97.1%	106
		<i>S. aureus</i>	93.7%	
Mesoporous $g\text{-C}_3\text{N}_4$	Hydrothermal	<i>E. coli</i>	Effective	107
$g\text{-C}_3\text{N}_4$ powder	Calcination	<i>E. coli</i>	Effective	108
		<i>S. epidermidis</i>		



in *E. coli* communities over the same time period. Additionally, under visible light, MCN-PVDF degrades the antibiotic cefotaxime (CFX) with a degradation rate of over 97% over five cycles.

When  $g\text{-C}_3\text{N}_4$  has a large specific surface area its photocatalytic performance is enhanced, e.g. in  $g\text{-C}_3\text{N}_4$  nanosheets and nanotubes, which have a high density active sites. Furthermore,  $g\text{-C}_3\text{N}_4$  nanocomposites inhibit  $e^-/h^+$  pair recombination and have high charge transfer efficiency due to enhanced visible light absorption. Hence, discrepant topologies of  $g\text{-C}_3\text{N}_4$  should have outstanding antibacterial performance and the discrepant

topologies of  $g\text{-C}_3\text{N}_4$ -based materials and their corresponding antibacterial properties are summarized in Table 1.

## 2.2 Noble metal decorated $g\text{-C}_3\text{N}_4$ nanocomposites

Another strategy used to increase the antibacterial performance of  $g\text{-C}_3\text{N}_4$  involves modification with noble metal nanoparticles, including silver and gold nanoparticles.<sup>109,110</sup> Surface Plasmon Resonance (SPR) of nanoparticles enhances antibacterial efficiency, by extending the spectral absorption range and promoting the formation of photogenerated carriers in  $g\text{-C}_3\text{N}_4$ .<sup>111–114</sup> Additionally, noble metal nanoparticles act as electron traps, capturing free  $e^-$  and thus inhibiting the

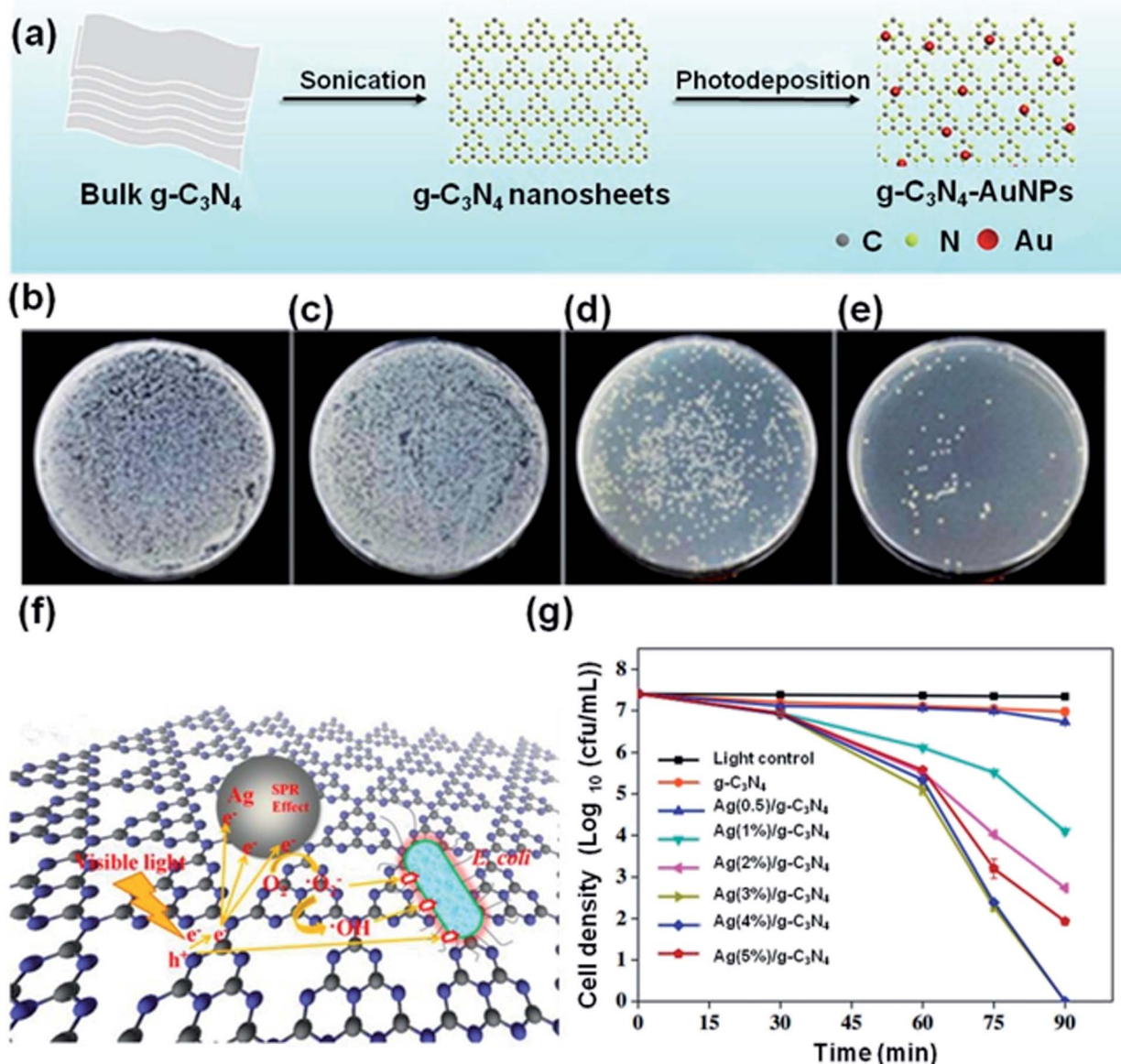


Fig. 5 (a) Preparation of  $g\text{-C}_3\text{N}_4\text{-Au}$  nanoparticle nanocomposites. (b) *E. coli* bacteria + control sample. (c) *E. coli* bacteria +  $g\text{-C}_3\text{N}_4$ -1.0% Au. (d) *E. coli* bacteria +  $g\text{-C}_3\text{N}_4$ -1.0% Au + 10 min irradiation. (e) *E. coli* bacteria +  $g\text{-C}_3\text{N}_4$ -1.0% Au + 20 min irradiation. Reproduced from ref. 123 with permission from American Chemical Society, copyright 2019. (f) The mechanism of *E. coli* inactivation in the presence of Ag/ $g\text{-C}_3\text{N}_4$  under visible light. (g) Disinfection efficiencies of *E. coli* by the samples under visible light irradiation. Reproduced from ref. 119 with permission from Elsevier, copyright 2019.



recombination of photogenerated carriers.<sup>115–118</sup> Ma *et al.* developed Ag/g-C<sub>3</sub>N<sub>4</sub> nanocomposites by combining thermal polymerization with photo-assisted reduction.<sup>119</sup> A synergistic antibacterial efficiency was achieved with superior sterilization activity of the Ag/g-C<sub>3</sub>N<sub>4</sub> nanocomposite compared to pure g-C<sub>3</sub>N<sub>4</sub> (Fig. 5f). Ag(0.3 wt%)/g-C<sub>3</sub>N<sub>4</sub> exhibited prominent antibacterial performance and suppressed *E. coli* replication (7.41 log) with only 1.25 h of visible light illumination. In contrast, pure g-C<sub>3</sub>N<sub>4</sub> displayed very low inactivation, with only about (0.4 log) *E. coli* killed following 1.5 h of illumination by visible light (Fig. 5g). Notably, the loading of noble Ag nanoparticles on the g-C<sub>3</sub>N<sub>4</sub> nanosheets significantly increases the visible light absorption region due to the SPR effect of the Ag nanoparticles and the charge transfer between the Ag and the g-C<sub>3</sub>N<sub>4</sub> nanosheets.<sup>120</sup> Similarly, the strong and unique surface plasmon resonance (SPR) absorption of gold nanoparticles covers a wide range of spectra, including the visible and near-infrared light (NIR).<sup>121,122</sup> As shown in Fig. 5a, Dai *et al.* utilized 5–10 nm sized Au nanoparticles to modify g-C<sub>3</sub>N<sub>4</sub> via liquid-phase exfoliation of g-C<sub>3</sub>N<sub>4</sub> combined with the photo-deposition of Au nanoparticles.<sup>123</sup> When a mixture of *E. coli* and the Au/g-C<sub>3</sub>N<sub>4</sub> nanocomposite were irradiated at 670 nm the resulting ROS effectively kill the bacteria. The viability of the bacteria continually diminishes over the illumination period (Fig. 5b–e). The incorporation of Au nanoparticles into the g-C<sub>3</sub>N<sub>4</sub> nanosheets strikingly improves photocatalytic ROS generation, due to the application of 670 nm light.<sup>124</sup> In general, noble metal/g-C<sub>3</sub>N<sub>4</sub> nanocomposites significantly outperform unmodified g-C<sub>3</sub>N<sub>4</sub> in antimicrobial experiments, and provide a viable photocatalytic disinfection method, see Table 2 for a summary.

### 2.3 Non-noble metal doped g-C<sub>3</sub>N<sub>4</sub> nanocomposites

While g-C<sub>3</sub>N<sub>4</sub> nanocomposites with noble metals have been shown to improve the photocatalytic antibacterial properties of the material, the high cost of noble metals prohibits widespread applications.<sup>125–129</sup> Thus, g-C<sub>3</sub>N<sub>4</sub> nanocomposites derived from inexpensive and abundant elements that are non-toxic would be advantageous.<sup>130–134</sup> In such materials the g-C<sub>3</sub>N<sub>4</sub> band gap may even be reduced to improve the separation efficiency of photo-generated carriers and the photoabsorption region may even be expanded to further improve the photocatalytic antibacterial performance.<sup>135–142</sup> Surface engineering of carbon-based materials has been an effective tool for construction of materials with special functions.<sup>143–149</sup> Advantageously, Lewis basic N-sites on the surface g-C<sub>3</sub>N<sub>4</sub> allow strong interactions with Lewis acids, *i.e.* zinc ions, similar to that observed for other materials.<sup>150–157</sup> For example, g-C<sub>3</sub>N<sub>4</sub>-Zn<sup>2+</sup>@graphene oxide (SCN-Zn<sup>2+</sup>@GO) were prepared using chemical vapor deposition (CVD).<sup>158</sup> The bidentate ligand, SCN, may coordinate to the Zn<sup>2+</sup> ions to form cross-links with GO, and additionally changing the crystal structure of g-C<sub>3</sub>N<sub>4</sub> and introducing defect sites (Fig. 6a). The resulting SCN-Zn<sup>2+</sup>@GO nanocomposite possessed excellent antibacterial activity. Irradiation at 808 nm (NIR) led to heating and irradiation at 660 nm resulted in the generation of ROS and the combination of photothermal and photodynamic processes effectively killed bacteria within a short time (almost quantitatively under the conditions employed). In Fig. 6b and d, the *E. coli* and *S. aureus* blank groups possess unbroken topologies, with glossy bacteria membranes and intact intra-cell structures. The membrane structures of both *E. coli* and *S. aureus* are ruptured under 808 nm and 660 nm light illumination. The intra-cell density decreases and part of cytoplasm overflows

Table 2 Antibacterial properties of noble metal decoration and non-noble metal doped g-C<sub>3</sub>N<sub>4</sub> nanocomposites

Main component	Material	Preparation	Bacteria	Effect	Ref.	
Noble metal decoration	Ag/g-C <sub>3</sub> N <sub>4</sub>	Thermal polymerization and photo-assisted reduction	<i>E. coli</i>	7.41 log	119	
	Ag/g-C <sub>3</sub> N <sub>4</sub>	Single-pot, microemulsion	<i>E. coli</i>	9.95 log	166	
	Ag/P/g-C <sub>3</sub> N <sub>4</sub>	Pyrolysis and green reduction.	<i>E. coli</i>	7 log	167	
	Ag/polydopamine/g-C <sub>3</sub> N <sub>4</sub>	Ultrasound and freeze-drying	<i>E. coli</i>	Effective	168	
	Ag/oxidized porous g-C <sub>3</sub> N <sub>4</sub>	Photo-assisted, reduction	<i>S. aureus</i>	99%	169	
	Ag/g-C <sub>3</sub> N <sub>4</sub>	Biogenic, methodology	<i>E. coli</i>	Effective	174	
			<i>S. aureus</i>			
			<i>P. aeruginosa</i>			
		Ag/g-C <sub>3</sub> N <sub>4</sub>	Calcination	<i>E. coli</i>	Effective	175
				<i>S. aureus</i>		
			<i>B. subtilis</i>			
			<i>P. aeruginosa</i>			
	Ag/g-C <sub>3</sub> N <sub>4</sub>	Photo-deposition method	<i>E. coli</i>	Effective	177	
			<i>P. aeruginosa</i>			
	Au/g-C <sub>3</sub> N <sub>4</sub>	Liquid-phase, exfoliation and photodeposition	<i>E. coli</i>	Effective	123	
	Au/g-C <sub>3</sub> N <sub>4</sub>	Deposition-precipitation	<i>E. coli</i>	82%	170	
			<i>S. aureus</i>	79%		
			<i>E. coli</i>	99%	176	
Non-noble metal doping	g-C <sub>3</sub> N <sub>4</sub> -Zn <sup>2+</sup> @graphene	Chemical vapor deposition and ultrasonic dispersion	<i>S. aureus</i>	99%	158	
	CQDs/g-C <sub>3</sub> N <sub>4</sub>	Impregnation	<i>S. aureus</i>	7 log	165	
	Fullerene/g-C <sub>3</sub> N <sub>4</sub>	Hydrothermal method	<i>E. coli</i> O157:H7	86%	171	
	S-CQD/hollow tubular g-C <sub>3</sub> N <sub>4</sub>	Self-assembly and ultrasound	<i>E. coli</i>	6.88 log	172	
	Ag/P/Co/S/g-C <sub>3</sub> N <sub>4</sub>	Calcination	<i>E. coli</i>	7 log	173	





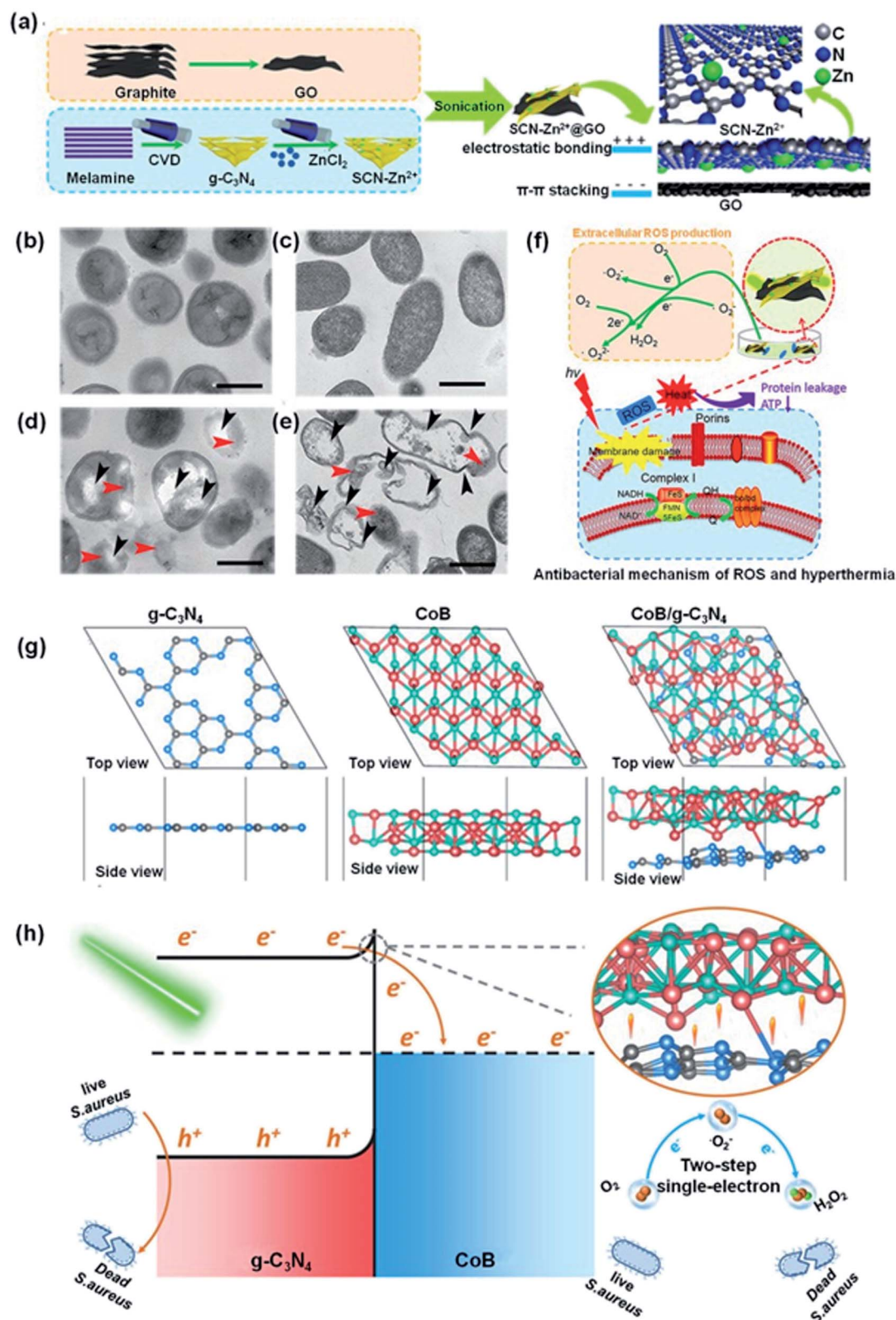


Fig. 6 (a) Preparation of SCN-Zn<sup>2+</sup>@GO. TEM topology of *S. aureus* (b) and *E. coli* (c) as control, (d) and (e) following treatment with SCN-Zn<sup>2+</sup>@GO 20% after 10 min irradiation with visible light (the red arrows indicate protein leakage and the dark arrows indicate rupture or ruffling of the bacterial membrane). (f) Antibacterial mechanism of SCN-Zn<sup>2+</sup>@GO 20% under 808 or 660 nm irradiation of ROS and hyperthermia. Reproduced from ref. 158 with permission from WILEY-VCH, copyright 2018. (g) Structural models of the g-C<sub>3</sub>N<sub>4</sub> (001) surface, CoB (010) surface and CoB/g-C<sub>3</sub>N<sub>4</sub> after geometry optimization. (h) The mechanism of *S. aureus* bacteria inactivation in the presence of CoB/g-C<sub>3</sub>N<sub>4</sub> under visible light. Reproduced from ref. 159 with permission from the American Chemical Society, copyright 2019.



Table 3 Antibacterial properties of g-C<sub>3</sub>N<sub>4</sub> heterojunction nanocomposites

Material	Preparation	Bacteria	Effect	Ref.
Bi <sub>2</sub> S <sub>3</sub> /g-C <sub>3</sub> N <sub>4</sub>	Ultrasound	<i>E. coli</i> <i>S. aureus</i>	99.6% 99.2%	185
Red P/g-C <sub>3</sub> N <sub>4</sub>	Sonochemical	<i>E. coli K-12</i>	7 log	186
Perylene diimide/oxygen-doped g-C <sub>3</sub> N <sub>4</sub>	<i>In situ</i> electrostatic assembling	<i>S. aureus</i>	99.6%	196
Bi <sub>2</sub> MoO <sub>6</sub> /g-C <sub>3</sub> N <sub>4</sub>	<i>In situ</i> solvothermal	<i>E. coli</i>	100%	199
MnO <sub>2</sub> /g-C <sub>3</sub> N <sub>4</sub>	Thermal vapor liquid-polymerization and redox	<i>E. coli</i> <i>S. aureus</i>	99.96% 99.26%	212
TiO <sub>2</sub> /kaolinite/g-C <sub>3</sub> N <sub>4</sub>	Sol-gel method	<i>S. aureus</i>	2.9 log	220
Ag/AgBr/g-C <sub>3</sub> N <sub>4</sub> /nitrogen-doped graphene aerogel	Hydrothermal and freeze-drying	<i>E. coli</i> <i>S. aureus</i>	~6 log ~1.2 log	252
Ag/AgBr/g-C <sub>3</sub> N <sub>4</sub>	<i>In situ</i> deposition-precipitation	<i>E. coli</i>	7.9 log	253
Ag <sub>2</sub> WO <sub>4</sub> /g-C <sub>3</sub> N <sub>4</sub>	Ultrasound	<i>E. coli</i>	90%	222
Ag <sub>2</sub> PO <sub>4</sub> /g-C <sub>3</sub> N <sub>4</sub>	Co-precipitation and thermal pyrolysis	<i>E. coli</i> <i>S. aureus</i>	Effective	254
Ni <sub>2</sub> P/g-C <sub>3</sub> N <sub>4</sub>	<i>In situ</i> anchoring and hydrothermal	<i>E. coli K-12</i>	7 log	255
<i>m</i> -Bi <sub>2</sub> O <sub>4</sub> /g-C <sub>3</sub> N <sub>4</sub>	Hydrothermal	<i>E. coli K-12</i>	6 log	223
Vanadium modified g-C <sub>3</sub> N <sub>4</sub> /TiO <sub>2</sub>	Calcination and ultrasonic	<i>E. coli</i> <i>S. aureus</i>	Effective	256
BiVO <sub>4</sub> /Ag/g-C <sub>3</sub> N <sub>4</sub>	Photodeposition and hydrothermal	<i>E. coli</i>	6.5 log	225
Ag/ZnO/g-C <sub>3</sub> N <sub>4</sub>	Thermal polymerization and solvothermal	<i>E. coli</i>	7.4 log	226
Ag/ZnO/g-C <sub>3</sub> N <sub>4</sub>	Thermal polymerization and solvothermal	<i>E. coli</i>	6.19 log	257
Ag <sub>2</sub> WO <sub>4</sub> /Ag/g-C <sub>3</sub> N <sub>4</sub>	Hydrothermal and <i>in situ</i> reductive	<i>E. coli</i>	3.05 log	258
Bi <sub>2</sub> MoO <sub>6</sub> -Ag/g-C <sub>3</sub> N <sub>4</sub>	Hydrothermal method	<i>E. coli</i> <i>S. aureus</i>	Effective	259
α-Fe <sub>2</sub> O <sub>3</sub> /CeO <sub>2</sub> /g-C <sub>3</sub> N <sub>4</sub>	Hydrothermal method	<i>E. coli</i> <i>S. aureus</i>	Effective	260
CuS/g-C <sub>3</sub> N <sub>4</sub>	Electrostatic adsorption	<i>E. coli</i> <i>S. aureus</i>	99% 98%	250
Vanadate QDs/g-C <sub>3</sub> N <sub>4</sub>	Sol-gel method	<i>Salmonella H9812</i>	96%	251
BiOI/g-C <sub>3</sub> N <sub>4</sub>	<i>In situ</i> generation	<i>E. coli</i> <i>S. aureus</i>	96% 98%	261
Cu <sub>2</sub> O/g-C <sub>3</sub> N <sub>4</sub>	Chemical precipitation	<i>E. coli</i>	7 log	262
Cu <sub>2</sub> O/g-C <sub>3</sub> N <sub>4</sub>	Hydrothermal method	<i>E. coli</i> <i>S. aureus</i>	Effective	263
TiO <sub>2</sub> nanofibers/Ag/g-C <sub>3</sub> N <sub>4</sub>	Ultrasound	<i>E. coli</i> <i>S. aureus</i>	99% 83%	264
Ag/AgCl/g-C <sub>3</sub> N <sub>4</sub>	<i>In situ</i> implanting and anchoring	Tetracycline-resistant bacteria	100%	265
γ-Fe <sub>2</sub> O <sub>3</sub> /Ag/AgCl/g-C <sub>3</sub> N <sub>4</sub>	Solvothermal and photodeposition	<i>E. coli</i>	5.59 log	266
RGO/CA/g-C <sub>3</sub> N <sub>4</sub>	Ultrasonification	<i>E. coli</i>	6.5 log	267
TiO <sub>2</sub> /CuBA/g-C <sub>3</sub> N <sub>4</sub>	Ultrasound	<i>E. coli</i> <i>S. aureus</i>	Effective	268
Ag <sub>2</sub> ZrO <sub>3</sub> /g-C <sub>3</sub> N <sub>4</sub>	Co-precipitation	<i>E. coli</i> <i>B. subtilis</i>	97% 99%	189
AgBr/g-C <sub>3</sub> N <sub>4</sub>	Adsorption deposition	<i>E. coli</i>	6.5 log	269
BiFeO <sub>3</sub> /Cu <sub>2</sub> O/g-C <sub>3</sub> N <sub>4</sub>	Hydrothermally and ultrasonic	<i>E. coli</i> <i>S. aureus</i>	Effective	270
ZnO/g-C <sub>3</sub> N <sub>4</sub> /cellulose	Ultrasonic irradiation	<i>E. coli</i> <i>S. aureus</i>	Effective	271
CdS/g-C <sub>3</sub> N <sub>4</sub>	Sonochemical	<i>E. coli</i> <i>S. aureus</i>	Effective	272
GO/g-C <sub>3</sub> N <sub>4</sub>	Sonication	<i>E. coli</i>	97.9%	70
AgCl/CNTs/g-C <sub>3</sub> N <sub>4</sub>	Deposition-precipitation	<i>E. coli</i>	Effective	273
MoO <sub>3-x</sub> /g-C <sub>3</sub> N <sub>4</sub>	Hydrothermal	<i>E. coli</i>	100%	274
AgO/g-C <sub>3</sub> N <sub>4</sub>	Chemical oxidation	<i>S. aureus</i>	89%	275
Fe-2,5-thiophenedicarboxylic acid/g-C <sub>3</sub> N <sub>4</sub>	Microwave-heating	<i>E. coli</i>	100%	276
Mg <sub>1.2</sub> Ti <sub>1.8</sub> O <sub>5</sub> /g-C <sub>3</sub> N <sub>4</sub>	Sol-gel method and calcination	<i>E. coli</i>	100%	277
CuWO <sub>4</sub> /g-C <sub>3</sub> N <sub>4</sub>	Sol-gel method	<i>E. coli</i> <i>S. aureus</i>	Effective	278
ZnBi <sub>2</sub> O <sub>4</sub> /g-C <sub>3</sub> N <sub>4</sub>	Ultrasound-assisted chemical exfoliation	<i>E. coli</i> <i>S. aureus</i>	Effective	279
Cr-ZnO/g-C <sub>3</sub> N <sub>4</sub>	Chemical coprecipitation method	<i>E. coli</i> <i>S. aureus</i>	Effective	280





Table 3 (Contd.)

Material	Preparation	Bacteria	Effect	Ref.
ZnBi <sub>2</sub> O <sub>4</sub> /g-C <sub>3</sub> N <sub>4</sub>	Thermal polycondensation	<i>B. subtilis</i> <i>E. coli</i>	97%	281
TiO <sub>2</sub> /Ag/g-C <sub>3</sub> N <sub>4</sub>	Vacuum freeze-drying	<i>E. coli</i>	84%	282
AgBr/g-C <sub>3</sub> N <sub>4</sub>	Calcination	<i>P. putida</i>	100%	283
TiO <sub>2</sub> nanotubes/Ti/g-C <sub>3</sub> N <sub>4</sub> /SnO <sub>2</sub>	Dipping and calcination	<i>E. coli</i>	Effective	284
BiOCl/g-C <sub>3</sub> N <sub>4</sub>	Hydrothermal method	<i>E. coli</i>	96%	285
NiFe <sub>2</sub> O <sub>4</sub> /g-C <sub>3</sub> N <sub>4</sub>	Hydrothermal method	<i>A. flavus</i>	90%	286
Perylene-3,4,9,10-tetracarboxylic diimide/g-C <sub>3</sub> N <sub>4</sub>	<i>In situ</i>	<i>E. coli</i> <i>S. aureus</i>	Effective	287
TiO <sub>2</sub> /g-C <sub>3</sub> N <sub>4</sub>	<i>In situ</i>	<i>E. coli</i>	65%	288
ZnO/Mn/g-C <sub>3</sub> N <sub>4</sub>	Chemical co-precipitation	<i>E. coli</i> <i>S. aureus</i>	Effective	289
ZnTiO <sub>2</sub> /S/g-C <sub>3</sub> N <sub>4</sub>	<i>In situ</i>	<i>E. coli</i> <i>S. aureus</i>	Effective	290
Ag-ZnO@g-C <sub>3</sub> N <sub>4</sub>	Physical mixing method	<i>E. coli</i> <i>S. aureus</i> <i>B. subtilis</i>	Effective	291
Poly(vinyl alcohol)/g-C <sub>3</sub> N <sub>4</sub>	Casting	<i>P. aeruginosa</i>	Effective	292
Polyaniline/g-C <sub>3</sub> N <sub>4</sub>	<i>In situ</i> oxidative polymerization methodology	<i>E. coli</i> <i>S. pneumoniae</i>	Effective	293
PVA/Starch/Ag@TiO <sub>2</sub> /g-C <sub>3</sub> N <sub>4</sub>	Solution casting	<i>E. coli</i> <i>S. aureus</i>	Effective	294
Fe@ZnO/g-C <sub>3</sub> N <sub>4</sub>	Chemical co-precipitation	<i>E. coli</i> <i>S. aureus</i> <i>B. subtilis</i> <i>S. salivarius</i>	Effective	295
g-C <sub>3</sub> N <sub>4</sub> -based metal-free	Calcination	<i>E. coli</i> <i>B. subtilis</i>	Effective	296
Ag <sub>2</sub> S/g-C <sub>3</sub> N <sub>4</sub>	Sonochemical	<i>E. coli</i> <i>S. aureus</i> <i>B. subtilis</i> <i>S. salivarius</i>	Effective	297
TiO <sub>2</sub> nanofibers/g-C <sub>3</sub> N <sub>4</sub>	Electrospinning-calcination	<i>E. coli</i> <i>S. aureus</i>	100%	298
Ag <sub>3</sub> PO <sub>4</sub> /g-C <sub>3</sub> N <sub>4</sub>	Hydrothermal method	<i>E. coli</i>	Effective	299
Ag <sub>2</sub> O/g-C <sub>3</sub> N <sub>4</sub>	Chemical deposition method	<i>M. aeruginosa</i>	99%	300
TiO <sub>2</sub> /g-C <sub>3</sub> N <sub>4</sub>	Hydrothermal and calcination	<i>E. coli</i>	100%	301
Ag <sub>2</sub> O/g-C <sub>3</sub> N <sub>4</sub>	Physical mixing method	<i>M. aeruginosa</i>	100%	302
AgO/g-C <sub>3</sub> N <sub>4</sub>	<i>In situ</i>	<i>E. coli</i>	Effective	303
Ag <sub>3</sub> PO <sub>4</sub> /g-C <sub>3</sub> N <sub>4</sub>	Hydrothermal method	<i>Bacteriophage f2</i>	100%	304
AgBr/g-C <sub>3</sub> N <sub>4</sub>	<i>In situ</i>	<i>E. coli</i>	100%	305
TiO <sub>2</sub> /g-C <sub>3</sub> N <sub>4</sub>	Hydrothermal	<i>E. coli</i>	100%	306
Porphyrin/g-C <sub>3</sub> N <sub>4</sub>	<i>In situ</i>	<i>S. aureus</i>	63%	307
Ag/Ag/Ag/g-C <sub>3</sub> N <sub>4</sub> /BiVO <sub>4</sub>	<i>In situ</i>	<i>E. coli</i>	100%	308
ZnO-Cd/g-C <sub>3</sub> N <sub>4</sub>	<i>In situ</i>	<i>E. coli</i> <i>S. aureus</i>	Effective	309
RGO/S <sub>8</sub> /g-C <sub>3</sub> N <sub>4</sub>	<i>In situ</i>	<i>E. coli K-12</i>	100%	310

(Fig. 6c and e, red arrows indicate protein or intra-cell material leakage and the black arrows indicate bacterial membrane distortion). In comparison, when SCN-Zn<sup>2+</sup>@GO was exposed to either 808 nm or 660 nm illumination, the inactivation rate obtained was only 20–66%. Based on the above results, the antibacterial mechanism is proposed in Fig. 6f. The ROS pass through the cell membrane of the bacteria to oxidize intracellular proteins and interfere homeostasis, while hyperthermia weakens the activities of the proteins and reduces adenosine triphosphate synthesis, inactivating *E. coli* and *S. aureus* within 10 min. Similarly, novel CoB/g-C<sub>3</sub>N<sub>4</sub> nanosheets were successfully prepared by an electrostatic self-assembly process coupled

with calcination.<sup>159</sup> The interfacial Co-N bond could act as an e<sup>-</sup> transport channel by accelerating the e<sup>-</sup> transfer from g-C<sub>3</sub>N<sub>4</sub> to CoB, as supported by density functional theory (DFT) calculations and indirectly evidenced from antibacterial experiments (Fig. 6g). Consequently, the e<sup>-</sup> induced O<sub>2</sub> reduction process is promoted in CoB/g-C<sub>3</sub>N<sub>4</sub>, which boosts the generation of ROS (Fig. 6h). Notably, CoB/g-C<sub>3</sub>N<sub>4</sub> exhibited superior disinfection efficacy of 100% against *S. aureus* with 125 min under visible light irradiation.

Quantum dots (QDs) are an important low-dimensional semiconductor materials. Because of their high reactivity and strong charge transfer abilities, QDs have been applied in



photocatalytic sterilization.<sup>160</sup> Carbon quantum dots (CQDs) were combined with  $g\text{-C}_3\text{N}_4$  to enhance charge transfer and store  $e^-$ .<sup>161–164</sup> Tang *et al.* constructed a CQD/ $g\text{-C}_3\text{N}_4$  photocatalyst by impregnation.<sup>165</sup> The addition of CQDs dramatically increased the disinfection performance, which was attributed to the increased ROS levels. The CQD/ $g\text{-C}_3\text{N}_4$  nanocomposites exhibit a greatly enhanced bactericidal efficiency under illumination with visible light. In contrast, the CQDs alone showed no catalytic activity against *S. aureus* under comparable conditions. Hence, the interaction between the CQDs and  $g\text{-C}_3\text{N}_4$  plays a significant role in increasing the bacterial inactivation efficiency.

#### 2.4 $g\text{-C}_3\text{N}_4$ heterojunction nanocomposites

Heterojunctions could enable the directional migration of photoinduced charges, allowing the charge to be enriched in specific direction, a process that should reduce or even inhibit the recombination of photogenerated carriers.<sup>178,179</sup> The antimicrobial properties of different  $g\text{-C}_3\text{N}_4$  heterojunctions are discussed, including type I and type II heterojunctions, p–n heterojunctions, and Z-scheme heterojunctions.<sup>180–184</sup> The photocatalytic antibacterial properties of  $g\text{-C}_3\text{N}_4$  heterojunction nanocomposites are listed in Table 3.

**2.4.1 Type I heterojunction nanocomposites.** In general, type I heterojunctions are rarely considered as the optimal choice in photocatalysis because the photogenerated carriers can transfer to the interface with other semiconductors, reducing the redox capacity of the charge carriers. Nevertheless, under visible light irradiation, type I heterojunctions have the unique advantage, *i.e.* the  $e^-$  and  $h^+$  can be transferred from one semiconductor to another. If another semiconductor has a wide photoabsorption window, a broad-spectrum-response photocatalyst with minimal charge recombination can be obtained by creating a type I heterojunction (Fig. 7a). Li *et al.* developed zinc-doped  $g\text{-C}_3\text{N}_4$  ( $g\text{-C}_3\text{N}_4\text{-Zn}$ ) with  $\text{Bi}_2\text{S}_3$  nanorod heterojunctions ( $g\text{-C}_3\text{N}_4\text{-Zn/BiS}$ ), using ultrasonication.<sup>185</sup> In contrast to the precursors ( $g\text{-C}_3\text{N}_4\text{-Zn}$  and  $\text{BiS}$ ), effective charge separation at the photocatalyst interface is achieved by adjusting the band gap, the density of the electronic distribution, and the oxygen adsorption capacity of the  $g\text{-C}_3\text{N}_4\text{-Zn/BiS}$  heterojunction. DFT calculations were employed to predict the stable crystal structure and the interface space between  $\text{CN-Zn}$  and  $\text{BiS}$  (Fig. 8a). The  $e^-$  and  $h^+$  were separated effectively by the energy band offset and the interface electric field, hence the  $g\text{-C}_3\text{N}_4\text{-Zn/BiS}$  heterojunction produces abundant ROS and shows excellent photocatalytic efficiency. Near-quantitative bactericidal efficiency towards *S. aureus* was achieved after only 10 min of NIR



Fig. 7 Various types of heterojunctions. (a) Type I heterojunction model. (b) Type II heterojunction model. (c) Z-type heterojunction model. (d) p–n heterojunction model.





Fig. 8 (a) Structural models of g-C<sub>3</sub>N<sub>4</sub>, g-C<sub>3</sub>N<sub>4</sub>-Zn, BiS, and g-C<sub>3</sub>N<sub>4</sub>-Zn/BiS after geometry optimization. (b) TEM topology of *S. aureus* after treatment with control or g-C<sub>3</sub>N<sub>4</sub>-Zn/BiS after 10 min irradiation. The white arrows indicate twisted and broken cell membranes and the blue arrows point to intracellular matrix outflow. Reproduced from ref. 185 with permission from WILEY-VCH, copyright 2019.

irradiation (Fig. 8b). In addition, red P was a novel single-element photocatalyst, and its visible light response range is up to 700 nm. Efficient light harvesting is imperative for photocatalysts, and with this in mind Wang *et al.* developed a wide-spectral-response g-C<sub>3</sub>N<sub>4</sub>/red P photocatalyst using ultrasound.<sup>186–188</sup> Ultrasonication was used to obtain nanosheets from bulk g-C<sub>3</sub>N<sub>4</sub>, and red P particles were anchored to the g-C<sub>3</sub>N<sub>4</sub> nanosheets to construct close g-C<sub>3</sub>N<sub>4</sub>/red P heterojunctions. g-C<sub>3</sub>N<sub>4</sub>/red P may form a new wide-spectral-responsive photocatalytic system to fully utilize the solar energy. In addition, g-C<sub>3</sub>N<sub>4</sub>/red P was used as a dual activity center photocatalyst, exhibiting dramatically improved photocatalytic efficiency for sterilization under illumination with visible light. While the g-C<sub>3</sub>N<sub>4</sub>/red P nanocomposite showed 7 log cfu mL<sup>-1</sup> bacterial inactivation after 1.3 h, the photocatalytic bacterial inactivation of pure g-C<sub>3</sub>N<sub>4</sub> was limited, with < 1.5 log cfu mL<sup>-1</sup> *E. coli* inactivation after 2 h of illumination.

**2.4.2 Type II heterojunction nanocomposites.** Type II heterojunctions g-C<sub>3</sub>N<sub>4</sub>-based nanocomposites have been widely reported as photocatalysts, *e.g.* Ag<sub>2</sub>ZrO<sub>3</sub>/g-C<sub>3</sub>N<sub>4</sub>,<sup>189</sup> Nb<sub>2</sub>O<sub>5</sub>/g-C<sub>3</sub>N<sub>4</sub> and Bi<sub>2</sub>MoO<sub>6</sub>/g-C<sub>3</sub>N<sub>4</sub>.<sup>190,191</sup> These materials have interlaced band gaps and appropriate VB and CB energies. Staggered heterojunctions are the most efficient type of heterojunctions due to highly efficient charge transfer,<sup>192–194</sup> and therefore, type II heterojunctions are widely used.<sup>195</sup> Exposure of a type II heterojunction to visible light results in the transition of an e<sup>-</sup> from the VB to the CB, generating a corresponding h<sup>+</sup> in the VB. When the CB of semiconductor A is higher in energy than the

CB of semiconductor B, the e<sup>-</sup> in the CB of semiconductor A is transferred to the CB of semiconductor B. Simultaneously, the h<sup>+</sup> in the VB of semiconductor B is transferred to the VB of semiconductor A. Finally, they react with O<sub>2</sub> and H<sub>2</sub>O in the surrounding media to produce ROS, leading to good antibacterial effects (Fig. 7b). Gao *et al.* prepared a perylene diimide (PDI)/oxygen-doped g-C<sub>3</sub>N<sub>4</sub> nanosheet (PDI/O-g-C<sub>3</sub>N<sub>4</sub>) nanocomposites using an *in situ* electrostatic assembly method.<sup>196</sup> The PDI expanded the visible light range of the material, resulting in abundant photogenerated charge carriers and accumulation of ROS, boosting the oxidative capability. As a consequence, PDI/O-g-C<sub>3</sub>N<sub>4</sub> demonstrated strong antibacterial oxidation activity under visible light with 96% of the *S. aureus* fully inactivated by PDI/O-g-C<sub>3</sub>N<sub>4</sub> under 3 h of light irradiation, whereas only 62% of the *S. aureus* cells were inactivated by the control material. Coincidentally, Bi<sub>2</sub>MoO<sub>6</sub> not only intersects the g-C<sub>3</sub>N<sub>4</sub> band gap, but also has a very similar band gap energy (~2.7 eV). Consequently, Bi<sub>2</sub>MoO<sub>6</sub> combines with g-C<sub>3</sub>N<sub>4</sub> to afford neoteric and efficient nanocomposites.<sup>197,198</sup> As shown in Fig. 9a, Li *et al.* developed Bi<sub>2</sub>MoO<sub>6</sub>/g-C<sub>3</sub>N<sub>4</sub> heterojunctions using an *in situ* solvothermal approach.<sup>199</sup> The results showed that the photocatalyst completely inactivated 2.5 × 10<sup>7</sup> cfu mL<sup>-1</sup> *E. coli* after 3 h light irradiation (Fig. 9b).

**2.4.3 Z-scheme heterojunction nanocomposites.** Recently, Z-scheme heterojunctions have been widely studied as the structure accelerates the separation of photogenerated carriers. The e<sup>-</sup> in the VB of semiconductor A transfers to the CB of





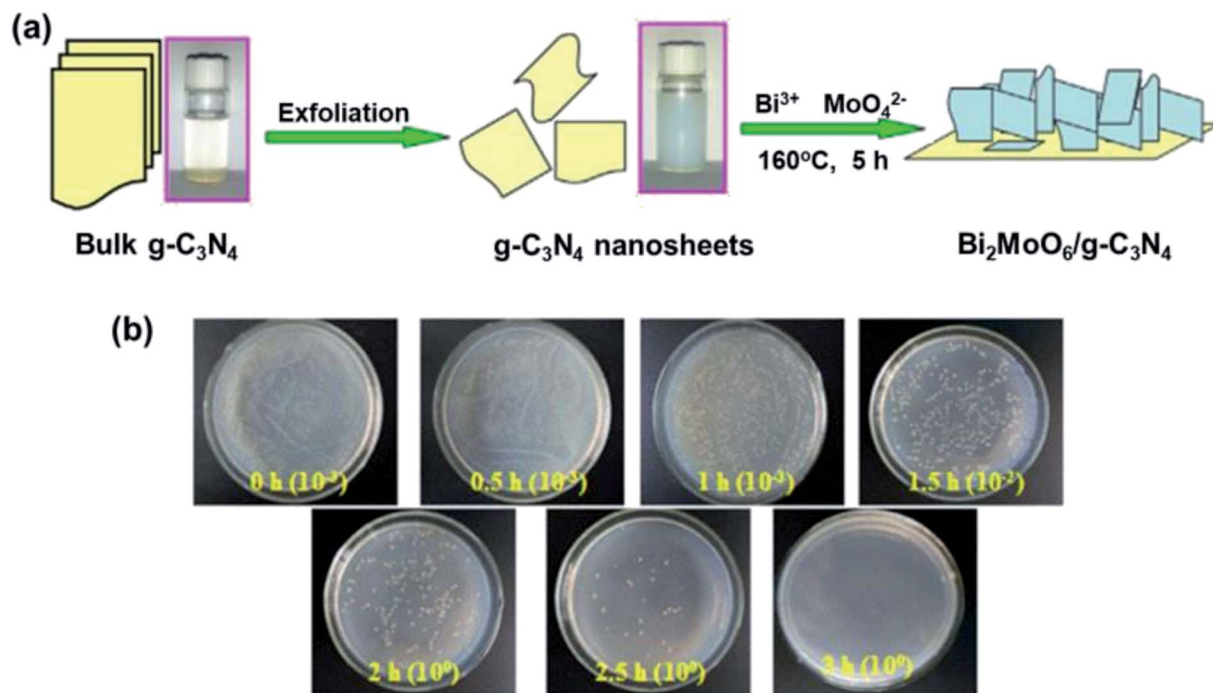
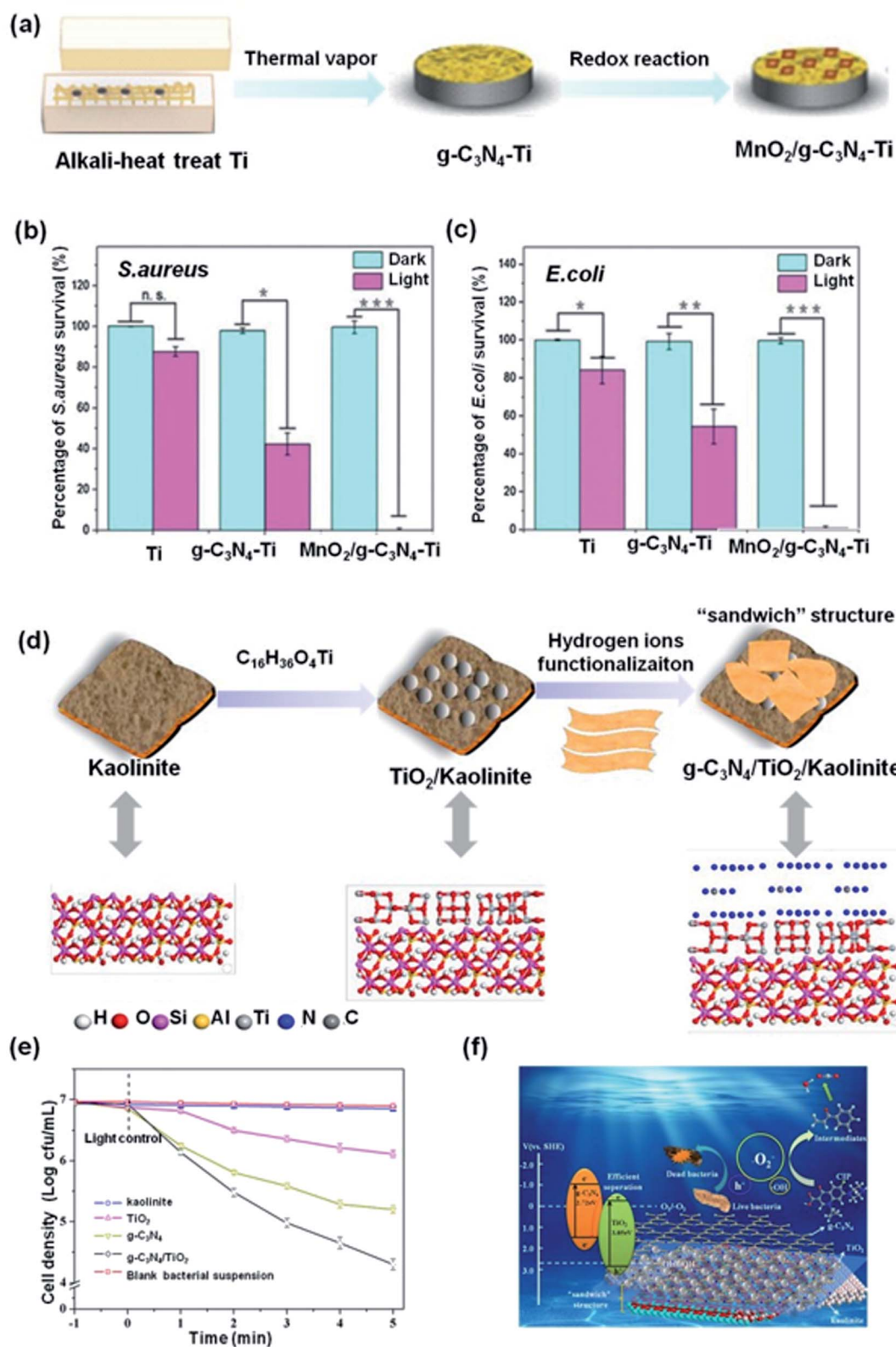


Fig. 9 (a) Preparation of the  $\text{Bi}_2\text{MoO}_6/\text{g-C}_3\text{N}_4$  heterojunction. (b) *E. coli* re-cultured after treatment with 20%  $\text{Bi}_2\text{MoO}_6/\text{g-C}_3\text{N}_4$  as a function of time. Reproduced from ref. 199 with permission from Elsevier, copyright 2016.

semiconductor B, and the remaining  $\text{h}^+$  and  $\text{e}^-$  undergo redox reactions with the oxygen and water in the surroundings to generate ROS (Fig. 7c). As expected, Z-scheme heterojunctions exhibit excellent photocatalytic disinfection performance.<sup>200–204</sup>  $\text{MnO}_2$  is an inexpensive, abundant, biocompatible semiconductor that has a similar bandgap to  $\text{g-C}_3\text{N}_4$ .<sup>205–211</sup> Wu *et al.* successfully constructed a  $\text{MnO}_2/\text{g-C}_3\text{N}_4\text{-Ti}$  heterojunction using thermal vapor liquid-polymerization and redox methods<sup>212</sup> (Fig. 10a). Contact between the  $\text{g-C}_3\text{N}_4$  and  $\text{MnO}_2$  formed a Z-scheme heterojunction. The  $\text{MnO}_2/\text{g-C}_3\text{N}_4\text{-Ti}$  composite inactivates *S. aureus* and *E. coli* in near-quantitative yields (Fig. 10b and c). In addition,  $\text{TiO}_2$  is an outstanding photocatalyst that binds with  $\text{g-C}_3\text{N}_4$  for form a nanocomposite with high thermal stability.<sup>213–219</sup> Li *et al.* constructed a  $\text{g-C}_3\text{N}_4/\text{TiO}_2/\text{kaolinite}$  heterojunction using a sol-gel approach combined with self-assembly<sup>220</sup> (Fig. 10d). Compared to bulk  $\text{g-C}_3\text{N}_4$  or  $\text{TiO}_2$ , the 3D structured  $\text{g-C}_3\text{N}_4/\text{TiO}_2/\text{kaolinite}$  nanocomposite displayed increased adsorption-photocatalytic sterilization of *S. aureus* under light irradiation. The  $\text{g-C}_3\text{N}_4/\text{TiO}_2/\text{kaolinite}$  composite inactivated 2.9 log *S. aureus* bacteria after 5 h of illumination, superior to  $\text{g-C}_3\text{N}_4$  (1.6 log) and  $\text{TiO}_2$  (0.8 log) alone (Fig. 10e). In addition, under visible light, the  $\text{g-C}_3\text{N}_4/\text{TiO}_2/\text{kaolinite}$  nanocomposite exhibits heightened adsorption-photocatalytic degradation of ciprofloxacin, a broad-spectrum antibiotic. The antibacterial efficiency of the  $\text{g-C}_3\text{N}_4/\text{TiO}_2/\text{kaolinite}$  composite may be attributed to both the improved light utilization and an increase in  $\text{e}^-$  transfer and separation efficiency (Fig. 10f). The visible light activated  $\text{g-C}_3\text{N}_4/\text{TiO}_2/\text{kaolinite}$  composite is a useful material for pollutant decomposition and bacterial elimination.<sup>221</sup>

**2.4.4 Dual-path heterojunction nanocomposites.** Generally, the charge migration paths observed in  $\text{g-C}_3\text{N}_4$  heterojunctions are mostly type II and Z-scheme heterojunctions, which expedite the fast separation of photogenerated charges and intensify the antibacterial activity of semiconductor materials. Many type II and Z-scheme heterojunction nanocomposites have been shown to inactivate bacteria under irradiation with visible light, including  $\text{m-Bi}_2\text{O}_4/\text{g-C}_3\text{N}_4$ ,  $\text{AgWO}_4/\text{g-C}_3\text{N}_4$ .<sup>222,223</sup> Nevertheless, due to the relatively low redox potentials in type II and Z-scheme heterojunctions, these photocatalysts lack strong redox abilities.<sup>224</sup> It is known that  $\text{e}^-$  accumulate in the CB of semiconductor A, which has a high reduction potential, and  $\text{h}^+$  leave the VB of semiconductor B, which has a high oxidation potential. This not only effectively separates the  $\text{e}^-/\text{h}^+$  pairs, but also produces the optimal redox properties. Therefore, the two models of ternary heterojunctions were also studied to further improve the antibacterial performance of photocatalytic heterojunctions. Zeng *et al.* constructed a ternary  $\text{BiVO}_4/\text{Ag}/\text{g-C}_3\text{N}_4$  heterojunction using photo-deposition and hydrothermal methods.<sup>225</sup> Based on heterojunction band gap energy level and surface chemistry, a dual Z-scheme photogenerated carrier transfer model was applied to  $\text{BiVO}_4/\text{Ag}/\text{g-C}_3\text{N}_4$ . Notably, the ternary  $\text{BiVO}_4/\text{Ag}/\text{g-C}_3\text{N}_4$  heterojunction markedly strengthened the photocatalytic antibacterial capability, completely inactivating 6.5 log *E. coli* cells after 1 h of light illumination, whereas the binary  $\text{BiVO}_4/\text{g-C}_3\text{N}_4$  heterojunction inactivated only 0.5 log *E. coli* under comparable conditions. The Ag and  $\text{BiVO}_4$  nanoparticles on the  $\text{g-C}_3\text{N}_4$  nanosheets inhibit recombination of the photogenerated carriers, thus promoting ROS generation. Ma *et al.* developed





**Fig. 10** (a) Schematic showing the preparation of  $\text{MnO}_2/\text{g-C}_3\text{N}_4\text{-Ti}$ . (b and c) The antibacterial effect of  $\text{MnO}_2/\text{g-C}_3\text{N}_4\text{-Ti}$  irradiated for 20 minutes against *S. aureus* and *E. coli*, respectively. Reproduced from ref. 212 with permission from Elsevier, copyright 2019. (d) Schematic illustration of the preparation of  $\text{g-C}_3\text{N}_4/\text{TiO}_2/\text{kaolinite}$ . (e) Photocatalytic disinfection efficiency of *S. aureus* for different samples. (f) Schematic diagram of photocatalytic mechanism of the  $\text{g-C}_3\text{N}_4/\text{TiO}_2/\text{kaolinite}$ . Reproduced from ref. 220 with permission from Elsevier, copyright 2019.



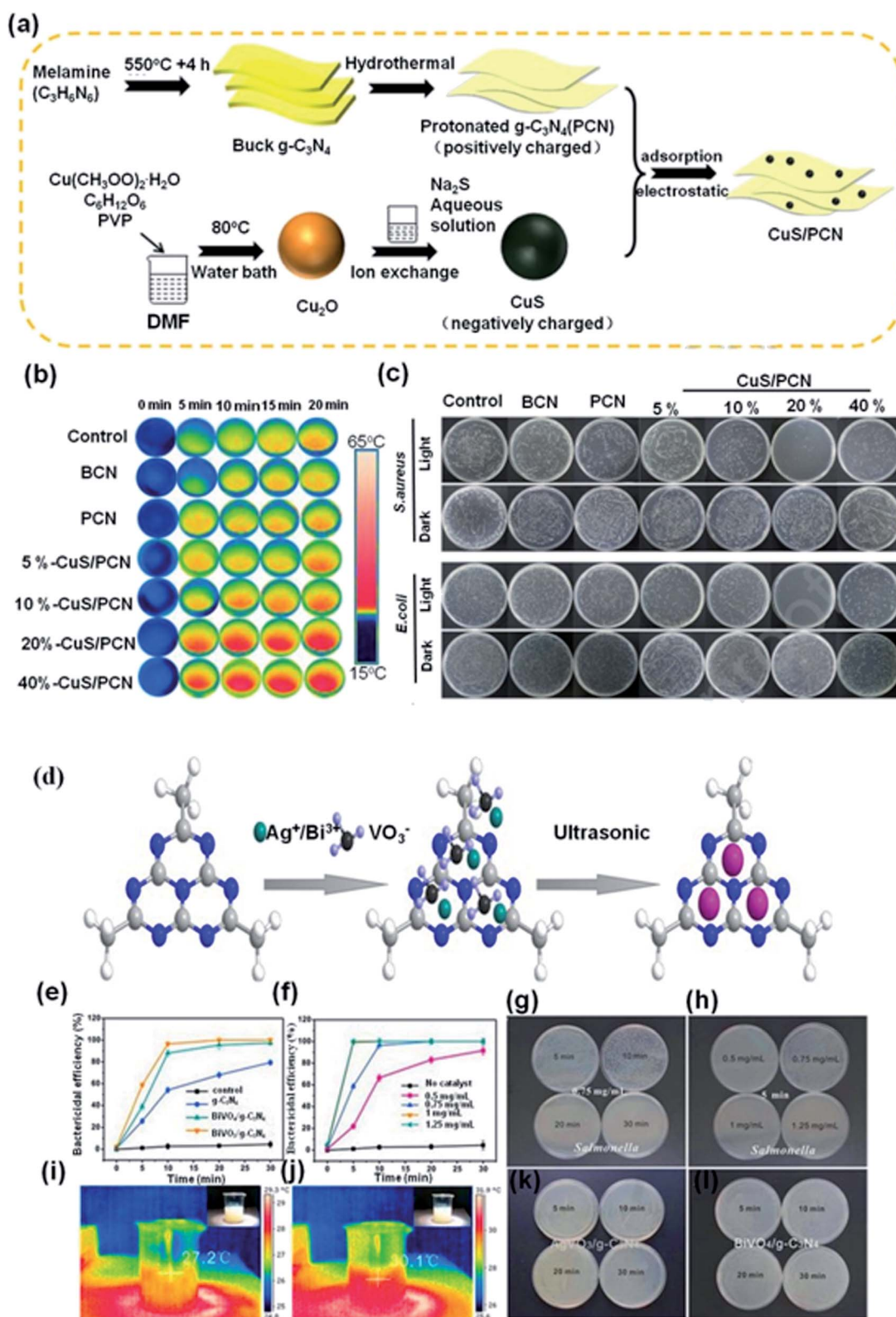


**Fig. 11** (a) Preparation of CuS/g-C<sub>3</sub>N<sub>4</sub>. (b) Photothermal images following irradiation as a function of concentration and time. (c) *In vitro* antibacterial activity for *S. aureus* and *E. coli*. Reproduced from ref. 250 with permission from Elsevier, copyright 2020. (d) Formation mechanism of vanadate QDs/g-C<sub>3</sub>N<sub>4</sub>. (e) Photocatalytic disinfection efficiency of *Salmonella* with different samples. (f) Photocatalytic disinfection efficiency of *Salmonella* with AgVO<sub>3</sub>/g-C<sub>3</sub>N<sub>4</sub> at different concentrations. (g) Bacteria colony growth in the presence of AgVO<sub>3</sub>/g-C<sub>3</sub>N<sub>4</sub> with *Salmonella*. (h) Bacteria colony growth in the presence of AgVO<sub>3</sub>/g-C<sub>3</sub>N<sub>4</sub> with *Salmonella* at different concentrations. The corresponding thermal images of AgVO<sub>3</sub>/g-C<sub>3</sub>N<sub>4</sub> following irradiation for (i) 5 min and (j) 10 min. Bacteria colony growth with (k) AgVO<sub>3</sub>/g-C<sub>3</sub>N<sub>4</sub> and (l) BIVO<sub>3</sub>/g-C<sub>3</sub>N<sub>4</sub> in the dark. Reproduced from ref. 251 with permission from Elsevier, copyright 2017.





ZnO/Ag/g-C<sub>3</sub>N<sub>4</sub> heterojunction using a solvothermal reaction.<sup>226</sup> This composite was used to kill *E. coli* under illumination with visible light. The ZnO/Ag/g-C<sub>3</sub>N<sub>4</sub> composite demonstrated significant visible light sterilization efficiency compared to g-C<sub>3</sub>N<sub>4</sub>, Ag/g-C<sub>3</sub>N<sub>4</sub> and ZnO/g-C<sub>3</sub>N<sub>4</sub> materials. Specifically, ZnO/Ag/g-C<sub>3</sub>N<sub>4</sub> inactivated 7.4 log *E. coli* after 2 h light illumination. However, only 0.49 log and 2.61 log *E. coli* were inactivated by g-C<sub>3</sub>N<sub>4</sub> and ZnO/g-C<sub>3</sub>N<sub>4</sub>. The interface of ZnO improves the sterilization performance by increasing the separation rate of charges because of the SPR effect of Ag and the similar band gap energies of ZnO to g-C<sub>3</sub>N<sub>4</sub>.<sup>227–231</sup>

**2.4.5 p–n heterojunction nanocomposites.** The construction of p–n type heterojunctions can increase the spectral response range of photocatalytic semiconductors.<sup>232–234</sup> The p–n type heterojunction needs to form at the interface of the space charge region and these heterojunctions form an internal potential that guides the e<sup>−</sup> and h<sup>+</sup> in opposite directions.<sup>235–239</sup> The e<sup>−</sup> transfers to the CB of the n-type semiconductor, whereas the h<sup>+</sup> transfers to the VB of the p-type semiconductor (Fig. 7d). The separation effect of charges in p–n heterojunctions is higher than other heterojunctions leading to superior photocatalytic antibacterial activity.<sup>240–245</sup> CuS is a p-type semiconductor and is the material of choice for photocatalysis due to its narrow band gap and excellent physicochemical stability.<sup>246–249</sup> Ding *et al.* synthesized CuS/g-C<sub>3</sub>N<sub>4</sub> heterojunction using a hydrothermal approach harnessing electrostatic adhesion.<sup>250</sup> In the CuS/g-C<sub>3</sub>N<sub>4</sub> heterojunction (Fig. 11a), the e<sup>−</sup> and h<sup>+</sup> transfer in reverse directions between g-C<sub>3</sub>N<sub>4</sub> and CuS, accelerating the separation of charges, thus producing high levels of ROS and increasing the photocatalytic antibacterial activity. In addition, the CuS/g-C<sub>3</sub>N<sub>4</sub> heterojunction can transform visible light to heat (Fig. 11b). Hence, due to the synergistic influence of the ROS and thermal effects, the CuS/g-C<sub>3</sub>N<sub>4</sub> composite inactivated *E. coli* and *S. aureus* bacteria near-quantitatively after 20 min of light irradiation. In contrast, g-C<sub>3</sub>N<sub>4</sub> only inactivated 30% of the *E. coli* cells and 25% of the *S. aureus* cells (Fig. 11c).

Wang *et al.* fabricated vanadate (AgVO<sub>3</sub> and BiVO<sub>4</sub>) QD/g-C<sub>3</sub>N<sub>4</sub> nanocomposites using urea<sup>251</sup> (Fig. 11d). Due to the abundant production of ROS by the vanadate QDs and g-C<sub>3</sub>N<sub>4</sub>, the vanadate QDs/g-C<sub>3</sub>N<sub>4</sub> composites exhibited high bactericidal efficiency, with 96% inactivation (AgVO<sub>3</sub> QDs/g-C<sub>3</sub>N<sub>4</sub>) and 87% inactivation (BiVO<sub>4</sub> QDs/g-C<sub>3</sub>N<sub>4</sub>) of *Salmonella* after only 10 min of light illumination (Fig. 11e and g). As shown in Fig. 11f and h, the photocatalytic disinfection efficiency increases with increasing photocatalyst concentration. Only 22% of *Salmonella* were killed with a AgVO<sub>3</sub>/g-C<sub>3</sub>N<sub>4</sub> composite concentration of 0.5 mg mL<sup>−1</sup>. However, at the same period, the photocatalytic inactivation of *Salmonella* increased to 58% when the photocatalyst concentration reach 0.75 mg mL<sup>−1</sup>. It is apparent from Fig. 11i and j that there is no significant change in temperature during the antibacterial tests. Furthermore, the bacteria grew well on the LB plate, meaning that photocatalyst does not kill the *Salmonella* (Fig. 11k and l). Considering the simplicity of the synthetic process, the chemical durability and the sterilization results, vanadate QDs/g-C<sub>3</sub>N<sub>4</sub> are ideal photocatalysts for applications in environmental settings.

### 3. Conclusions and perspectives

Materials based on g-C<sub>3</sub>N<sub>4</sub> are promising photocatalysts with excellent physico-chemical properties and have considerable promise in antibacterial applications. Nevertheless, the antibacterial applications of bulk g-C<sub>3</sub>N<sub>4</sub> are limited by its narrow absorption of visible light and facile recombination of charges. Consequently, a variety of g-C<sub>3</sub>N<sub>4</sub>-based nanocomposites have been developed with high superficial areas, improved e<sup>−</sup>/h<sup>+</sup> separation efficiencies and expanded visible light absorption ranges, combining to enhance their antibacterial activity. In this review, we highlighted the main strategies used to amplify the photocatalytic efficiency of g-C<sub>3</sub>N<sub>4</sub>-based nanocomposites and their antimicrobial properties, including different topologies, noble metal decoration, non-noble metal doping and heterojunction construction. The enhancement mechanisms and synergistic effects of g-C<sub>3</sub>N<sub>4</sub>-based nanocomposites was also discussed. Although g-C<sub>3</sub>N<sub>4</sub> is an ideal photocatalyst for the construction of nanocomposites for antibacterial applications, there are still some issues to be solved and opportunities for further research:

(1) The antibacterial mechanism of g-C<sub>3</sub>N<sub>4</sub>-based nanocomposites include destroying cell membranes and cell walls, producing endotoxins, causing protein mutations, interfering with protein synthesis and oxidizing organics. However, the role of each process in the antibacterial activity has not yet been clearly defined, suggesting that future research on the antibacterial mechanisms of g-C<sub>3</sub>N<sub>4</sub>-based nanocomposites would be meaningful.

(2) Although g-C<sub>3</sub>N<sub>4</sub>-based nanocomposites have been extensively studied, the photocatalytic properties are not always predictable, and the performance between g-C<sub>3</sub>N<sub>4</sub> and co-composites is often found to be additive and not synergistic. Therefore, molecular models that allow better composite design would be useful.

(3) When constructing g-C<sub>3</sub>N<sub>4</sub> heterojunctions, a single heterojunction has many limitations in terms of light absorption and e<sup>−</sup> separation. Thus, the construction of dual heterojunctions, such as dual Z-type or combined Z-type and type II heterojunctions could enhance the photocatalytic effect of g-C<sub>3</sub>N<sub>4</sub> nanocomposites and is a key topic for future research and development.

(4) The antibacterial efficiency of g-C<sub>3</sub>N<sub>4</sub>-based nanocomposite photocatalysts relies largely on ultraviolet and blue light. Extending the range to longer wavelengths would be advantageous.

(5) Most studies were carried at laboratory scales and synthetic strategies for large-scale production are challenging. The development of simple and large-scale green and sustainable synthetic methods that can be automated are required to facilitate commercial applications.

(6) ROS are also able to destroy viruses and therefore further research exploring the antiviral properties of g-C<sub>3</sub>N<sub>4</sub> nanocomposites would be valuable.

### Conflicts of interest

There are no conflicts to declare.



## Acknowledgements

This work was supported by the National Natural Science Foundation of China (51803112, 216740859), China Postdoctoral Science Foundation Grant (2018M633503), Key Laboratory Construction Program of Xi'an Municipal Bureau of Science and Technology (201805056ZD7CG40), and Innovation Capability Support Program of Shaanxi (No. 2018PT-28, 2019PT-05).

## References

- 1 R. Edwards and K. G. Harding, *Curr. Opin. Infect. Dis.*, 2004, **17**, 91–96.
- 2 J. Bures, J. Cyrany, D. Kohoutova, M. Förstl, S. Rejchrt, J. Kvetina, V. Vorisek and M. Kopacova, *World J. Gastroenterol.*, 2010, **16**, 2978.
- 3 T. Wei, Q. Yu and H. Chen, *Adv. Healthcare Mater.*, 2019, **8**, 1801381.
- 4 Y. Elad, H. Yunis and T. Katan, *Plant Pathol.*, 1992, **41**, 41–46.
- 5 K. Su, L. Tan, X. M. Liu, Z. D. Cui, Y. F. Zheng, B. Li, Y. Han, Z. Y. Li, S. L. Zhu, Y. Q. Liang, X. B. Feng, X. B. Wang and S. L. Wu, *ACS Nano*, 2020, **14**, 2077–2089.
- 6 X. Z. Xie, C. Y. Mao, X. M. Liu, Y. Z. Zhang, Z. D. Cui, X. J. Yang, K. W. K. Yeung, H. B. Pan, P. K. Chu and S. L. Wu, *ACS Appl. Mater. Interfaces*, 2017, **9**, 26417–26428.
- 7 U. Tsutomu, Y. Tetsuya, T. Sigeru and A. Keisuke, *Chem. Lett.*, 2003, **32**, 330–331.
- 8 L. H. Li, J. C. Deng, H. R. Deng, Z. L. Liu and X. L. Li, *Chem. Eng. J.*, 2010, **160**, 378–382.
- 9 F. B. Liu, S. C. Lai, H. J. Tong, P. S. J. Lakey, M. Shiraiwa, M. G. Weller, U. Poschl and C. J. Kampf, *Anal. Bioanal. Chem.*, 2017, **409**, 2411–2420.
- 10 Q. Li, T. Li, C. Liu, G. Deloid, G. Pyrgiotakis, P. Demokritou, R. Zhang, H. Xiao and D. J. McClements, *Nanotoxicology*, 2017, **11**, 1–15.
- 11 K. Yan, Y. B. Zhang, C. L. Mu, Q. N. Xu, X. N. Jing, D. Q. Wang, D. F. Dang, L. J. Meng and J. Z. Ma, *Theranostics*, 2020, **10**, 7287–7318.
- 12 X. N. Jing, Z. Zhi, N. Zhang, H. H. Song, Y. Z. Xu, G. Q. Zhou, D. Q. Wang, Y. P. Shao and L. J. Meng, *Chem. Eng. J.*, 2020, **385**, 123893.
- 13 J. S. Ni, T. L. Min, Y. X. Li, M. L. Zha, P. F. Zhang, C. L. Ho and K. Li, *Angew. Chem., Int. Ed.*, 2020, **59**, 10179–10185.
- 14 L. S. R. Yadav, K. Manjunath, C. Kavitha and G. Nagaraju, *J. Sci.: Adv. Mater. Devices*, 2018, **3**, 181–187.
- 15 K. Ghule, A. V. Ghule, B. J. Chen and Y. C. Ling, *Green Chem.*, 2006, **8**, 1034–1041.
- 16 C. Y. Mao, Y. M. Xiang, X. M. Liu, Z. D. Cui, X. J. Yang, Z. Y. Li, K. W. K. Yeung, H. Pan, X. B. Wang, P. K. Chu and S. L. Wu, *ACS Nano*, 2017, **11**, 9010–9021.
- 17 F. He, G. Chen, Y. G. Yu, S. Hao, Y. S. Zhou and Y. Zheng, *ACS Appl. Mater. Interfaces*, 2014, **6**, 7171–7179.
- 18 J. W. Fu, J. G. Yu, C. J. Jiang and B. Cheng, *Adv. Energy Mater.*, 2018, **8**, 1701503.
- 19 J. Q. Wen, J. Xie, X. B. Chen and X. Li, *Appl. Surf. Sci.*, 2017, **391**, 72–123.
- 20 T. Xiong, W. L. Cen, Y. X. Zhang and F. Dong, *ACS Catal.*, 2016, **6**, 2462–2472.
- 21 Z. S. Chen, S. Zhang, Y. Liu, N. S. Alharbi, S. O. Rabah, S. H. Wang and X. X. Wang, *Sci. Total Environ.*, 2020, **731**, 139054.
- 22 S. Kumar, S. Karthikeyan and A. F. Lee, *Catalysts*, 2018, **8**, 74.
- 23 W. K. Darkwah and Y. H. Ao, *Nanoscale Res. Lett.*, 2018, **13**, 388.
- 24 Y. Xu and S. P. Gao, *Int. J. Hydrogen Energy*, 2012, **37**, 11072–11080.
- 25 C. Prasad, H. Tang, Q. Q. Liu, I. Bahadur, S. Karlapudi and Y. J. Jiang, *Int. J. Hydrogen Energy*, 2020, **45**, 337–379.
- 26 X. Y. Lu, J. Xie, X. B. Chen and X. Li, *Appl. Catal., B*, 2019, **252**, 250–259.
- 27 L. T. Ma, H. Q. Fan, K. Fu, S. H. Lei, Q. Z. Hu, H. T. Huang and G. P. He, *ACS Sustainable Chem. Eng.*, 2017, **5**, 7093–7103.
- 28 Y. Zhao, J. Zhang and L. T. Qu, *ChemNanoMat*, 2015, **1**, 298–318.
- 29 A. Zambon, J. M. Mouesca, C. Gheorghiu, P. A. Bayle, J. Pécaut, M. C. Bruno, S. Gambarell and L. Dubois, *Chem. Sci.*, 2015, **7**, 945–950.
- 30 X. C. Wang, K. Maeda, A. Thomas, K. Takane, G. Xin, J. M. Carlsson, K. Domen and M. Antonietti, *Nat. Mater.*, 2009, **8**, 76–80.
- 31 A. Fujishima and K. Honda, *Nature*, 1972, **238**, 37–38.
- 32 L. M. Hu, J. T. Yan, C. L. Wang, B. Chai and J. F. Li, *Chin. J. Catal.*, 2019, **40**, 458–469.
- 33 X. Li, C. Y. Liu, D. Y. Wu, J. Z. Li, P. W. Huo and H. Q. Wang, *Chin. J. Catal.*, 2019, **40**, 928–939.
- 34 B. Chai, J. T. Yan, G. Z. Fan, G. S. Song and C. L. Wang, *Chin. J. Catal.*, 2020, **41**, 170–179.
- 35 Y. Li, X. Li, H. W. Zhang, J. J. Fan and Q. J. Xiang, *J. Mater. Sci. Nanotechnol.*, 2020, **56**, 69–88.
- 36 D. Q. Gao, Q. Xu, J. Zhang, Z. L. Yang, M. S. Si, Z. J. Yan and D. S. Xue, *Nanoscale*, 2014, **6**, 2577–2581.
- 37 M. Groenewolt and M. Antonietti, *Adv. Mater.*, 2005, **17**, 1789–1792.
- 38 B. C. Zhu, P. F. Xia, W. K. Ho and J. G. Yu, *Appl. Surf. Sci.*, 2015, **344**, 188–195.
- 39 H. N. Che, C. B. Liu, G. B. Che, G. F. Liao, H. J. Dong, C. X. Li, N. Song and C. M. Li, *Nano Energy*, 2020, **67**, 104273.
- 40 Z. Y. Wang, Y. Huang, M. J. Chen, X. J. Shi, Y. F. Zhang, J. J. Cao, W. K. Ho and S. C. Lee, *ACS Appl. Mater. Interfaces*, 2019, **11**, 10651–10662.
- 41 Y. D. Zou, B. B. Yang, Y. Liu, Y. Ren, J. H. Ma, X. R. Zhou, X. W. Cheng and Y. H. Deng, *Adv. Funct. Mater.*, 2018, **28**, 1806214.
- 42 Y. H. Li, M. L. Gu, M. Zhang, X. M. Zhang, K. L. Lv, W. K. Ho and F. Dong, *Chem. Eng. J.*, 2020, **389**, 124421.
- 43 Z. X. Sun, H. Q. Wang, Z. B. Wu and L. Z. Wang, *Catal. Today*, 2017, **300**, 160–172.
- 44 A. Nikokavoura and C. Trapalis, *Appl. Surf. Sci.*, 2018, **430**, 18–52.



- 45 F. He, Z. X. Wang, Y. X. Li, S. Q. Peng and B. Liu, *Appl. Catal., B*, 2020, **269**, 118828.
- 46 I. Papailias, N. Todorova, T. Giannakopoulou, N. Ioannidis, P. Dallas, D. Dimotikali and C. Trapalis, *Appl. Catal., B*, 2020, **268**, 118733.
- 47 D. D. Ren, Z. Z. Liang, Y. H. Ng, P. Zhang, Q. J. Xiang and X. Li, *Chem. Eng. J.*, 2020, **390**, 124496.
- 48 X. Li, J. Xie, C. J. Jiang, J. G. Yu and P. Y. Zhang, *Front. Environ. Sci. Eng.*, 2018, **12**, 14.
- 49 H. C. Lan, L. L. Li, X. Q. An, F. Liu, C. B. Chen, H. J. Liu and J. H. Qu, *Appl. Catal., B*, 2017, **204**, 49–57.
- 50 J. Y. Shan, K. L. Yang, W. J. Xiu, Q. Qiu, S. L. Dai, L. H. Yuwen, L. X. Weng, Z. G. Teng and L. H. Wang, *Small*, 2020, **16**, 2001099.
- 51 C. C. Han, P. F. Su, B. H. Tan, X. G. Ma, H. Lv, C. Y. Huang, P. Wang, Z. F. Tong, G. Li, Y. Z. Huang and Z. F. Liu, *J. Colloid Interface Sci.*, 2021, **581**, 159–166.
- 52 R. C. Shen, J. Xie, X. Y. Lu, X. B. Chen and X. Li, *ACS Sustainable Chem. Eng.*, 2018, **6**, 4026–4036.
- 53 R. C. Shen, J. Xie, P. Y. Guo, L. S. Chen, X. B. Chen and X. Li, *ACS Appl. Energy Mater.*, 2018, **1**, 2232–2241.
- 54 L. L. Sun, C. Y. Liu, J. Z. Li, Y. J. Zhou, H. Q. Wang, P. W. Huo, C. C. Ma and Y. S. Yan, *Chin. J. Catal.*, 2019, **40**, 80–94.
- 55 R. C. Shen, Y. N. Ding, S. B. Li, P. Zhang, Q. J. Xiang, Y. H. Ng and X. Li, *Chin. J. Catal.*, 2021, **42**, 25–36.
- 56 X. J. Bai, L. Wang, R. L. Zong and Y. F. Zhu, *J. Phys. Chem. C*, 2013, **117**, 9952–9961.
- 57 Z. X. Jiang, X. Zhang, H. S. Chen, X. Hu and P. Yang, *ChemCatChem*, 2019, **11**, 4558–4567.
- 58 B. Chong, L. Chen, D. Z. Han, L. Wang, L. J. Feng, Q. Li, C. H. Li and W. T. Wang, *Chin. J. Catal.*, 2019, **40**, 959–968.
- 59 R. C. Shen, K. L. He, A. P. Zhang, N. Li, Y. H. Ng, P. Zhang, J. Hu and X. Li, *Appl. Catal., B*, 2021, **291**, 120104.
- 60 R. Geng, J. J. Yin, J. X. Zhou, T. F. Jiao, Y. Feng, L. X. Zhang, Y. Chen, Z. H. Bai and Q. M. Peng, *Nanomaterials*, 2020, **10**, 1.
- 61 X. Y. Chu, Y. Qu, A. Zada, L. L. Bai, Z. J. Li, F. Yang, L. N. Zhao, G. L. Zhang, X. J. Sun, Z. D. Yang and L. Q. Jing, *Adv. Sci.*, 2020, **7**, 2001543.
- 62 X. G. Ma, Y. H. Lv, J. Xu, Y. F. Liu, R. Q. Zhang and Y. F. Zhu, *J. Phys. Chem. C*, 2012, **116**, 23485–23493.
- 63 J. W. Fu, B. C. Zhu, C. J. Jiang, B. Cheng, W. You and J. G. Yu, *Small*, 2017, **13**, 1603938.
- 64 S. C. Yan, Z. S. Li and Z. G. Zou, *Langmuir*, 2010, **26**, 3894–3901.
- 65 Y. F. Li, M. H. Zhou, B. Cheng and Y. Shao, *J. Mater. Sci. Nanotechnol.*, 2020, **56**, 1–17.
- 66 J. Y. Li, Z. Y. Zhang, W. Cui, H. Wang, W. L. Cen, G. Johnson, G. M. Jiang, S. Zhang and F. Dong, *ACS Catal.*, 2018, **8**, 8376–8385.
- 67 R. C. Shen, D. D. Ren, Y. N. Ding, Y. T. Guan, Y. H. Ng, P. Zhang and X. Li, *Sci. China Mater.*, 2020, **63**, 2153–2188.
- 68 S. Z. Butler, S. M. Hollen, L. Y. Cao, Y. Cui, J. A. Gupta, H. R. Gutiérrez, T. F. Heinz, S. Sa. Hong, J. X. Huang, A. F. Ismach, E. J. Halperin, M. Kuno, V. V. Plashnitsa, R. D. Robinson, R. S. Ruoff, S. Salahuddin, J. Shan, L. Shi, M. G. Spencer, M. Terrones, W. Windl and J. E. G. Cao, *ACS Nano*, 2013, **7**, 2898–2926.
- 69 F. Dong, Z. Zhao, T. Xiong, Z. Ni, W. D. Zhang, Y. J. Sun and W. K. Ho, *ACS Appl. Mater. Interfaces*, 2013, **5**, 11392–11401.
- 70 L. Sun, T. Du, C. Hu, J. Chen, J. Lu, Z. Lu and H. Han, *ACS Sustainable Chem. Eng.*, 2017, **5**, 8693–8701.
- 71 Y. Wang, X. C. Wang and M. Antonietti, *Angew. Chem., Int. Ed.*, 2012, **51**, 68–89.
- 72 W. J. Ong, L. L. Tan, Y. H. Ng, S. T. Yong and S. P. Chai, *Chem. Rev.*, 2016, **116**, 7159–7329.
- 73 J. Wang, G. H. Wang, B. Cheng, J. G. Yu and J. J. Fan, *Chin. J. Catal.*, 2021, **42**, 56–68.
- 74 Y. L. Liu, S. S. Wu, J. Liu, S. B. Xie and Y. J. Liu, *RSC Adv.*, 2021, **11**, 4810–4817.
- 75 D. D. Ren, W. N. Zhang, Y. N. Ding, R. C. Shen, Z. M. Jiang, X. Y. Lu and X. Li, *Sol. RRL*, 2020, **4**, 1900423.
- 76 M. Tahir, C. B. Cao, F. K. Butt, F. Idrees, N. Mahmood, Z. Ali, I. Aslam, M. Tanveer, M. Rizwan and T. Mahmood, *J. Mater. Chem. A*, 2013, **1**, 13949–13955.
- 77 Z. W. Tong, D. Yang, Y. Y. Sun, Y. H. Nan and Z. Y. Jiang, *Small*, 2016, **12**, 4093–4101.
- 78 J. Y. Li, Z. Y. Zhang, W. Cui, H. Wang, W. L. Cen, G. Johnson, G. M. Jiang, S. Zhang and F. Dong, *ACS Catal.*, 2018, **8**, 8376–8385.
- 79 J. D. Hong, S. M. Yin, Y. X. Pan, J. Y. Han, T. H. Zhou and R. Xu, *Nanoscale*, 2014, **6**, 14984–14990.
- 80 Q. H. Liang, Z. Li, Z. H. Huang, F. Kang and Q. H. Yang, *Adv. Funct. Mater.*, 2015, **25**, 6885–6892.
- 81 Y. Jian, D. M. Wang, M. Z. Huang, H. L. Jia, J. H. Sun, X. K. Song and M. G. Guan, *ACS Sustainable Chem. Eng.*, 2017, **5**, 6827–6834.
- 82 R. Li, Y. L. Ren, P. X. Zhao, J. Wang, J. D. Liu and Y. T. Zhang, *J. Hazard. Mater.*, 2019, **365**, 606–614.
- 83 C. L. Fu, L. J. Meng, Q. H. Lu, Z. F. Fei and P. J. Dason, *Adv. Funct. Mater.*, 2008, **18**, 857.
- 84 Q. Li, J. P. Yang, D. Feng, Z. X. Wu, Q. L. Wu, S. S. Park, C. S. Ha and D. Y. Zhao, *Nano Res.*, 2010, **3**, 632–642.
- 85 J. Xu, Z. P. Wang and Y. F. Zhu, *J. Mater. Sci. Nanotechnol.*, 2020, **49**, 133–143.
- 86 Z. W. Tong, D. Yang, Z. Li, Y. H. Nan, F. Ding, Y. C. Shen and Z. Y. Jiang, *ACS Nano*, 2017, **11**, 1103–1112.
- 87 F. Yang, G. Y. Ding, J. Wang, Z. H. Liang, B. Gao, M. M. Dou, C. Xu and S. M. Li, *J. Membr. Sci.*, 2020, **606**, 118146.
- 88 I. Kohsari, Z. Shariatnia and S. M. Pourmortazavi, *Int. J. Biol. Macromol.*, 2016, **91**, 778–788.
- 89 J. Wang, Y. M. Wang, Y. T. Zhang, A. Uliana, J. Y. Zhu, J. D. Liu and B. V. Bruggen, *ACS Appl. Mater. Interfaces*, 2016, **8**, 25508–25519.
- 90 S. F. Kang, L. Zhang, M. F. He, Y. Y. Zheng, L. F. Cui, Di Sun and B. Hu, *Carbon*, 2018, **137**, 19–30.
- 91 J. Xu, Z. P. Wang and Y. F. Zhu, *ACS Appl. Mater. Interfaces*, 2017, **9**, 27727–27735.
- 92 S. F. Kang, W. Huang, L. Zhang, M. F. He, S. Y. Xu, D. Sun and X. Jiang, *ACS Appl. Mater. Interfaces*, 2018, **10**, 13796–13804.
- 93 J. H. Thurston, N. M. Hunter, L. J. Wayment and K. A. Cornell, *J. Colloid Interface Sci.*, 2017, **505**, 910–918.





- 94 N. N. He, S. H. Cao, L. H. Zhang, Z. D. Tian, H. Chen and F. J. Jiang, *Chemosphere*, 2019, **235**, 1116–1124.
- 95 Z. Y. Teng, N. L. Yang, H. Y. Lv, S. C. Wang, M. Z. Hu, C. Y. Wang, D. Wang and G. X. Wang, *Chem*, 2019, **5**, 664–680.
- 96 Y. Li, C. Zhang, D. M. Shuai, S. Naraginti, D. W. Wang and W. L. Zhang, *Water Res.*, 2016, **106**, 249–258.
- 97 J. Q. Chen, W. T. Lin, L. Y. Xie, J. H. Huang and W. J. Wang, *J. Nanomater.*, 2019, **2019**, 1–9.
- 98 P. Yadav, S. T. Nishanthi, B. Purohit, A. Shanavas and K. Kailasam, *Carbon*, 2019, **152**, 587–597.
- 99 Y. Li, Y. N. Li, S. L. Ma, P. F. Wang, Q. L. Hou, J. J. Han and S. H. Zhan, *J. Hazard. Mater.*, 2017, **338**, 33–46.
- 100 J. Xu, J. Huang, Z. P. Wang and Y. F. Zhu, *Chin. J. Catal.*, 2020, **41**, 474–484.
- 101 H. F. Li, M. N. Ding, L. L. Luo, G. X. Yang, F. Y. Shi and Y. N. Huo, *ChemCatChem*, 2020, **12**, 1334–1340.
- 102 N. Jiang, H. C. Geng, Y. Qiao, X. Q. Zhu, C. Y. Li and Q. Y. Cai, *New J. Chem.*, 2020, **44**, 2303–2311.
- 103 F. L. Wang, Y. P. Feng, P. Chen, Y. F. Wang, Y. H. Su, Q. X. Zhang, Y. Q. Zeng, Z. J. Xie, H. J. Liu, Y. Liu, W. Y. Lv and G. G. Liu, *Appl. Catal., B*, 2018, **227**, 114–122.
- 104 G. X. Song, L. W. Wang, R. Q. Yang, Y. C. Ji, R. T. Zhang, L. Yang, L. H. Ding, A. Z. Wang, N. Ren and X. Yu, *J. Nanosci. Nanotechnol.*, 2020, **20**, 5944–5950.
- 105 N. S. Heo, S. Shukla, S. Y. Oh, V. K. Bajpai, S. U. Lee, H. J. Cho, S. Kim, Y. Kim, H. J. Kim, S. Y. Lee, Y. S. Jun, M. H. Oh, Y. K. Han, S. M. Yoo and Y. S. Huh, *Mater. Sci. Eng.*, 2019, **104**, 109846.
- 106 J. H. Thurston, N. M. Hunter and K. A. Cornell, *RSC Adv.*, 2016, **6**, 42240–42248.
- 107 A. Mirzaei, Z. Chen, F. Haghghat and L. Yerushalmi, *Appl. Catal., B*, 2019, **242**, 337–348.
- 108 H. C. Shen, E. A. López-Guerra, R. C. Zhu, T. Diba, Q. M. Zheng, S. D. Solares, J. M. Zara, D. M. Shuai and Y. Shen, *ACS Appl. Mater. Interfaces*, 2019, **11**, 373–384.
- 109 S. F. Kang, Y. Fang, Y. K. Huang, L. F. Cui, Y. Z. Wang, H. F. Qin, Y. M. Zhang, X. Li and Y. G. Wang, *Appl. Catal., B*, 2015, **168**, 472–482.
- 110 S. Patnaik, D. P. Sahoo and K. Parida, *Renewable Sustainable Energy Rev.*, 2018, **82**, 1297–1312.
- 111 F. K. Meng, J. T. Li, S. K. Cushing, J. Bright, M. J. Zhi, J. D. Rowley, Z. L. Hong, A. Manivannan, A. D. Bristow and N. Q. Wu, *ACS Catal.*, 2013, **3**, 746–751.
- 112 L. J. Meng, W. J. Xia, L. Liu, L. Y. Niu and Q. H. Lu, *ACS Appl. Mater. Interfaces*, 2014, **6**, 4989–4996.
- 113 J. G. Mcevoy and Z. S. Zhang, *J. Photochem. Photobiol., C*, 2014, **19**, 62–75.
- 114 D. B. Ingram, P. Christopher, J. L. Bauer and S. Linic, *ACS Catal.*, 2011, **1**, 1441–1447.
- 115 Q. Q. Ding, R. Li, M. D. Chen and M. T. Sun, *Appl. Mater. Today*, 2017, **9**, 251–258.
- 116 S. H. Wang, J. W. Zhan, K. Chen, A. Ali, L. H. Zeng, H. Zhao, W. L. Hu, L. X. Zhu and X. L. Xu, *ACS Sustainable Chem. Eng.*, 2020, **8**, 8214–8222.
- 117 K. H. Sun, J. Shen, Q. Q. Liu, H. Tang, M. Y. Zhang, S. Zulfiqar and C. S. Lei, *Chin. J. Catal.*, 2020, **41**, 72–81.
- 118 Z. Q. Ren, F. Y. Chen, K. X. Wen and J. F. Lu, *J. Photochem. Photobiol., A*, 2020, **389**, 112217.
- 119 S. L. Ma, S. H. Zhan, Y. N. Jia, Q. Shi and Q. X. Zhou, *Appl. Catal., B*, 2016, **186**, 77–87.
- 120 X. J. Bai, R. L. Zong, C. X. Li, D. Liu, Y. F. Liu and Y. F. Zhu, *Appl. Catal., B*, 2014, **147**, 82–91.
- 121 L. J. Meng, L. Y. Niu, L. Li, Q. H. Lu, Z. F. Fei and P. J. Dyson, *Chem.–Eur. J.*, 2012, **18**, 13314–13319.
- 122 D. Q. Wang, L. J. Meng, Z. F. Fei, C. Hou, J. G. Long, L. L. Zeng, P. J. Dyson and P. Huang, *Nanoscale*, 2018, **10**, 8536–8546.
- 123 J. Y. Dai, J. B. Song, Y. Qiu, J. J. Wei, Z. Z. Hong, L. Li and H. H. Yang, *ACS Appl. Mater. Interfaces*, 2019, **11**, 10589–10596.
- 124 V. Shanmugam, S. Selvakumar and C. S. Yeh, *Chem. Soc. Rev.*, 2014, **43**, 6254–6287.
- 125 E. Atilla, S. K. Toprak and T. Demirer, *Turk. J. Haematol.*, 2017, **34**, 1–9.
- 126 Z. L. Jin and L. J. Zhang, *J. Mater. Sci. Nanotechnol.*, 2020, **49**, 144–156.
- 127 Z. Z. Liang, R. C. Shen, Y. H. Ng, P. Zhang, Q. J. Xiang and X. Li, *J. Mater. Sci. Nanotechnol.*, 2020, **56**, 89–121.
- 128 Y. T. Gao, F. Chen, Z. Chen and H. F. Shi, *J. Mater. Sci. Nanotechnol.*, 2020, **56**, 227–235.
- 129 K. Wang, Q. Li, B. S. Liu, B. Cheng, W. K. Ho and J. G. Yu, *Appl. Catal., B*, 2015, **176**, 44–52.
- 130 X. X. Zhao, J. R. Guan, J. Z. Li, X. Li, H. Q. Wang, P. W. Huo and Y. S. Yan, *Appl. Surf. Sci.*, 2021, **537**, 147891.
- 131 H. N. Che, G. B. Che, P. J. Zhou, C. B. Liu, H. J. Dong, C. X. Li, N. Song and C. M. Li, *Chem. Eng. J.*, 2020, **382**, 122870.
- 132 M. D. Capobianco, B. Pattengale, J. Neu and C. A. Schmuttenmaer, *J. Phys. Chem. Lett.*, 2020, **11**, 8873–8879.
- 133 X. Y. Lu, J. Xie, S. Y. Liu, A. Adamski, X. B. Chen and X. Li, *ACS Sustainable Chem. Eng.*, 2018, **6**, 13140–13150.
- 134 R. C. Shen, J. Xie, Q. J. Xiang, X. B. Chen, J. Z. Jiang and X. Li, *Chin. J. Catal.*, 2019, **40**, 240–288.
- 135 Y. P. Zhu, T. Z. Ren and Z. Y. Yuan, *ACS Appl. Mater. Interfaces*, 2015, **7**, 16850–16856.
- 136 G. Liu, P. Niu, C. H. Sun, S. C. Smith, Z. G. Chen, G. Q. Lu and H. M. Cheng, *J. Am. Chem. Soc.*, 2010, **132**, 11642–11648.
- 137 J. W. Fang, H. Q. Fan, M. M. Li and C. B. Long, *J. Mater. Chem. A*, 2015, **3**, 13819–13826.
- 138 N. Güy, *Appl. Surf. Sci.*, 2020, **522**, 146442.
- 139 Y. Wang, Y. Di, M. Antonietti, H. R. Li, X. F. Chen and X. C. Wang, *Chem. Mater.*, 2010, **22**, 5119–5121.
- 140 C. Zhou, R. Shi, L. Shang, L. Z. Wu, C. H. Tung and T. R. Zhang, *Nano Res.*, 2018, **11**, 3462–3468.
- 141 R. C. Shen, C. J. Jiang, Q. J. Xiang, J. Xie and X. Li, *Appl. Surf. Sci.*, 2019, **471**, 43–87.
- 142 Y. J. Li, L. Ding, Y. C. Guo, Z. Q. Liang, H. Z. Cui and J. Tian, *ACS Appl. Mater. Interfaces*, 2019, **11**, 41440–41447.
- 143 C. L. Fu, L. J. Meng, Q. H. Lu, X. K. Zhang and C. Gao, *Macromol. Rapid Commun.*, 2007, **28**, 2180–2184.



- 144 R. Xia, Z. F. Fei, N. Drigo, F. D. Bobbink, Z. J. Huang, R. Jasiunas, M. Franckevicius, V. Gulbinas, M. Mensi, X. D. Fang, C. R. Carmona, M. K. Nazeeruddin and P. J. Dyson, *Adv. Funct. Mater.*, 2019, **29**, 1902021.
- 145 J. T. Gao, Y. Wang, S. J. Zhou, W. Lin and Y. Kong, *ChemCatChem*, 2017, **9**, 1708–1715.
- 146 J. Q. Wen, J. Xie, H. D. Zhang, A. P. Zhang, Y. J. Liu, X. B. Chen and X. Li, *ACS Appl. Mater. Interfaces*, 2017, **9**, 14031–14042.
- 147 H. Tang, R. Wang, C. X. Zhao, Z. P. Chen, X. F. Yang, D. Bukhvalov, Z. X. Lin and Q. Q. Liu, *Chem. Eng. J.*, 2019, **374**, 1064–1075.
- 148 J. J. Feng, D. K. Zhang, H. P. Zhou, M. Y. Pi, X. D. Wang and S. J. Chen, *ACS Sustainable Chem. Eng.*, 2018, **6**, 6342–6349.
- 149 P. Sun, H. Liu, M. B. Feng, Z. C. Zhai, Y. S. Fang, X. S. Zhang and V. K. Sharma, *Appl. Catal., B*, 2020, **272**, 119005.
- 150 L. J. Meng, C. L. Fu, Z. F. Fei, Q. H. Lu and P. J. Dyson, *Inorg. Chim. Acta*, 2010, **363**, 3926–3931.
- 151 J. Ran, T. Pan, Y. Y. Wu, C. Q. Chu, P. Cui, P. P. Zhang, X. Y. Ai, C. F. Fu, Z. J. Yang and T. W. Xu, *Angew. Chem., Int. Ed.*, 2019, **58**, 16463–16468.
- 152 X. D. Du, X. H. Yi, P. Wang, J. G. Deng and C. C. Wang, *Chin. J. Catal.*, 2019, **40**, 70–79.
- 153 M. F. R. Samsudin, H. Ullah, A. A. Tahir, X. H. Li, Y. H. Ng and S. Sufian, *J. Colloid Interface Sci.*, 2021, **586**, 785–796.
- 154 Q. Yang, S. W. Yu, P. Fu, W. Yu, Y. Liu, X. Liu, Z. C. Feng, X. Guo and C. Li, *Adv. Funct. Mater.*, 2020, **30**, 1910205.
- 155 X. B. Li, J. Xiong, Y. Xu, Z. J. Feng and J. T. Huang, *Chin. J. Catal.*, 2019, **40**, 424–433.
- 156 C. Liu, Y. Feng, Z. T. Han, Y. Sun, X. Q. Wang, Q. F. Zhang and Z. G. Zou, *Chin. J. Catal.*, 2021, **42**, 164–174.
- 157 H. G. Yu, J. C. Xu, D. D. Gao, J. J. Fan and J. G. Yu, *Sci. China Mater.*, 2020, **63**, 2215–2227.
- 158 Y. Li, X. M. Liu, L. Tan, Z. D. Cui, X. J. Yang, Y. F. Zheng, K. W. K. Yeung, P. K. Chu and S. L. Wu, *Adv. Funct. Mater.*, 2018, **28**, 1800299.
- 159 H. Guo, C. G. Niu, Y. Y. Yang, C. Liang, H. Y. Niu, H. Y. Liu, L. Li and N. Tang, *Chem. Eng. J.*, 2021, **422**, 130029.
- 160 P. G. Sionnest, *Microchim. Acta*, 2008, **160**, 309–314.
- 161 X. Q. Wu, J. Zhao, S. J. Guo, L. P. Wang, W. L. Shi, H. Huang, Y. Liu and Z. H. Kang, *Nanoscale*, 2016, **8**, 17314–17321.
- 162 X. J. Yu, J. J. Liu, Y. C. Yu, S. L. Zuo and B. S. Li, *Carbon*, 2014, **68**, 718–724.
- 163 H. J. Feng, Q. Q. Guo, Y. F. Xu, T. Chen, Y. Y. Zhou, Y. G. Wang, M. Z. Wang and D. S. Shen, *Chemosuschem*, 2018, **11**, 4256–4261.
- 164 Y. Y. Li, Y. Fang, Z. L. Cao, N. J. Li, D. Y. Chen, Q. F. Xu and J. M. Lu, *Appl. Catal., B*, 2019, **250**, 150–162.
- 165 C. Y. Tang, C. Liu, Y. Han, Q. Q. Guo, W. Ouyang, H. J. Feng, M. Z. Wang and F. Xu, *Adv. Healthcare Mater.*, 2019, **8**, 1801534.
- 166 M. J. M. Batista, O. F. Carceller, M. Ferrer, M. F. García and A. Kubacka, *Appl. Catal., B*, 2016, **183**, 86–95.
- 167 P. She, J. Li, H. G. Bao, X. Q. Xu and Z. Hong, *J. Photochem. Photobiol., A*, 2019, **384**, 112028.
- 168 Y. Y. Wu, Y. Z. Zhou, H. Xu, Q. Q. Liu, Y. Li, L. L. Zhang, H. Q. Liu, Z. G. Tu, X. N. Cheng and J. Yang, *ACS Sustainable Chem. Eng.*, 2018, **6**, 14082–14094.
- 169 J. Xu, Q. Z. Gao, X. J. Bai, Z. P. Wang and Y. F. Zhu, *Catal. Today*, 2019, **332**, 227–235.
- 170 Z. Z. Wang, K. Dong, Z. Liu, Y. Zhang, Z. W. Chen, H. J. Sun, J. S. Ren and X. G. Qu, *Biomaterials*, 2017, **113**, 145–157.
- 171 K. Ouyang, K. Dai, H. Chen, Q. Y. Huang, C. H. Gao and P. Cai, *Ecotoxicol. Environ. Saf.*, 2017, **136**, 40–45.
- 172 W. J. Wang, Z. T. Zeng, G. M. Zeng, C. Zhang, R. Xiao, C. Y. Zhou, W. P. Xiong, Y. Yang, L. Lei, Y. Liu, D. L. Huang, M. Cheng, Y. Y. Yang, Y. K. Fu, H. Z. Luo and Y. Zhou, *Chem. Eng. J.*, 2019, **378**, 122132.
- 173 X. Q. Xu, S. M. Wang, X. F. Yu, J. L. Dawa, D. L. Gui and R. H. Tang, *Appl. Surf. Sci.*, 2020, **501**, 144245.
- 174 M. E. Khan, T. H. Han, M. M. Khan, M. R. Karim and M. H. Cho, *ACS Appl. Nano Mater.*, 2018, **1**, 2912–2922.
- 175 C. C. Liu, L. Wang, H. Xu, S. Wang, S. M. Gao, X. C. Ji, Q. Xu and W. Lan, *Mater. Lett.*, 2016, **164**, 567–570.
- 176 H. D. Zhang, X. Zhang, M. H. Zhu, H. Y. Li, Y. Zhao, X. R. Han, L. H. Jin and H. X. Shan, *ChemPlusChem*, 2020, **85**, 2722–2730.
- 177 Z. Y. Liu, M. Y. Zhang and J. L. Wu, *ChemistrySelect*, 2018, **3**, 10630–10636.
- 178 X. B. Chen, S. H. Shen, L. J. Guo and S. S. Mao, *Chem. Rev.*, 2010, **110**, 6503–6570.
- 179 S. I. Sadovnikov and A. I. Gusev, *J. Mater. Chem. A*, 2017, **5**, 17676–17704.
- 180 Y. X. Yan, H. Yang, Z. Yi, R. S. Li and T. Xian, *Solid State Sci.*, 2020, **100**, 106102.
- 181 N. N. Yuan, J. F. Zhang, S. J. Zhang, G. L. Chen, S. G. Meng, Y. Fan, X. Z. Zheng and S. F. Chen, *J. Phys. Chem. C*, 2020, **124**, 8561–8575.
- 182 Y. Y. Wang, H. L. Huang, Z. Z. Zhang, C. Wang, Y. Y. Yang, Q. Li and D. S. Xu, *Appl. Catal., B*, 2021, **282**, 119570.
- 183 C. J. Wang, Y. L. Zhao, H. Xu, Y. F. Li, Y. C. Wei, J. Liu and Z. Zhao, *Appl. Catal., B*, 2020, **263**, 118314.
- 184 E. V. Kermani, A. H. Yangjeh, H. D. Khalilabad and S. Ghosh, *J. Colloid Interface Sci.*, 2020, **563**, 81–91.
- 185 Y. Li, X. M. Liu, L. Tan, Z. D. Cui, D. D. Jing, X. J. Yang, Y. Q. Liang, Z. Y. Li, S. L. Zhu, Y. F. Zheng, K. W. K. Yeung, D. Zheng, X. B. Wang and S. L. Wu, *Adv. Funct. Mater.*, 2019, **29**, 1900946.
- 186 W. J. Wang, G. Y. Li, T. C. An, D. K. L. Chan, J. C. Yu and P. K. Wong, *Appl. Catal., B*, 2018, **238**, 126–135.
- 187 Y. P. Yuan, L. S. Yin, S. W. Cao, L. N. Gu, G. S. Xu, P. W. Du, H. Chai, Y. S. Liao and C. Xue, *Green Chem.*, 2014, **16**, 4663–4668.
- 188 L. Jing, R. X. Zhu, D. L. Phillips and J. C. Yu, *Adv. Funct. Mater.*, 2017, **46**, 1703484.
- 189 R. S. Das, S. K. Warkhade, A. Kumar, G. S. Gaikwad and A. V. Wankhade, *J. Alloys Compd.*, 2020, **846**, 155770.
- 190 I. Khan, N. Baig and A. Qurashi, *ACS Appl. Energy Mater.*, 2018, **2**, 607–615.
- 191 Y. Tian, F. Zhou, S. Zhan, Z. Y. Zhu and Q. C. He, *J. Photochem. Photobiol., A*, 2018, **350**, 10–16.



- 192 L. Y. Lu, G. H. Wang, M. Zou, J. Wang and J. Li, *Appl. Surf. Sci.*, 2018, **441**, 1012–1023.
- 193 Z. F. Huang, J. J. Song, X. Wang, L. Pan, K. Li, X. W. Zhang, L. Wang and J. J. Zou, *Nano Energy*, 2017, **40**, 308–316.
- 194 J. Wang, G. H. Wang, X. H. Wei, G. Liu and J. Li, *Appl. Surf. Sci.*, 2018, **456**, 666–675.
- 195 R. R. Hao, G. H. Wang, C. J. Jiang, H. Tang and Q. C. Xu, *Appl. Surf. Sci.*, 2017, **411**, 400–410.
- 196 Q. Z. Gao, J. Xu, Z. P. Wang and Y. F. Zhu, *Appl. Catal., B*, 2020, **15**, 118933.
- 197 F. Chen, C. G. Niu, Q. Yang, X. M. Li and G. M. Zeng, *Ceram. Int.*, 2016, **42**, 2515–2525.
- 198 L. W. Zhang, T. G. Xu, X. Zhao and Y. F. Zhu, *Appl. Catal., B*, 2010, **98**, 138–146.
- 199 J. Li, Y. C. Yin, E. Z. Liu, Y. N. Ma, J. Wan, J. Fan and X. Y. Hu, *J. Hazard. Mater.*, 2017, **321**, 183–192.
- 200 M. L. Tang, Y. H. Ao, C. Wang and P. F. Wang, *Appl. Catal., B*, 2020, **268**, 118395.
- 201 P. F. Chen, L. Chen, S. F. Ge, W. Q. Zhang, M. F. Wu, P. X. Xing, T. B. Rotamond, H. J. Lin, Y. Wu and Y. M. He, *Int. J. Hydrogen Energy*, 2020, **45**, 14354–14367.
- 202 S. Panimalar, R. Uthrakumar, E. T. Selvi, P. Gomathy, C. Inmozhi, K. Kaviyarasu and J. Kennedy, *Surf. Interfaces*, 2020, **20**, 100512.
- 203 Q. L. Xu, B. C. Zhu, C. J. Jiang, B. Cheng and J. G. Yu, *Sol. RRL*, 2018, **2**, 1800006.
- 204 P. F. Xia, B. C. Zhu, B. Cheng, J. G. Yu and J. S. Xu, *ACS Sustainable Chem. Eng.*, 2018, **6**, 965–973.
- 205 R. Millaleo, M. R. Diaz, A. G. Ivanov, M. L. Mora and M. Alberdi, *J. Soil Sci. Plant Nutr.*, 2010, **10**, 470–481.
- 206 B. Nanda, A. C. Pradhan and K. M. Parida, *Microporous Mesoporous Mater.*, 2016, **226**, 229–242.
- 207 Z. Y. Ma, Y. Sun, J. W. Xie, P. P. Li, Q. J. Lu, M. L. Liu, P. Yin, H. T. Li, Y. Y. Zhang and S. Z. Yao, *ACS Appl. Mater. Interfaces*, 2020, **12**, 15919–15927.
- 208 H. H. Zeng, B. L. Xing, C. T. Zhang, L. J. Chen, H. H. Zhao, X. F. Han, G. Y. Yi, G. X. Huang, C. X. Zhang and Y. J. Cao, *Energy Fuels*, 2020, **34**, 2480–2491.
- 209 X. Gao, H. W. Wu, W. J. Li, Y. Tian, Y. Zhang, H. Wu, L. Yang, G. Q. Zou, H. S. Hou and X. B. Ji, *Small*, 2020, **16**, 1905842.
- 210 Z. H. Huang, Y. Song, D. Y. Feng, Z. Sun, X. Q. Sun and X. X. Liu, *ACS Nano*, 2018, **12**, 3557–3567.
- 211 F. F. Wu, X. B. Gao, X. L. Xu, Y. N. Jiang, X. L. Gao, R. L. Yin, W. H. Shi, W. X. Liu, G. Lu and X. H. Cao, *ChemSusChem*, 2020, **13**, 1537–1545.
- 212 B. B. Wu, Y. Li, K. Su, L. Tan, X. M. Liu, Z. D. Cui, X. J. Yang, Y. Q. Liang, Z. Y. Li, S. L. Zhu, K. W. K. Yeung and L. S. Wu, *J. Hazard. Mater.*, 2019, **377**, 227–236.
- 213 L. M. Sun, X. Zhao, C. J. Jia, Y. X. Zhou, X. F. Cheng, P. Li, L. Liu and W. L. Fan, *J. Mater. Chem.*, 2012, **22**, 23428–23438.
- 214 C. Q. Li, Z. M. Sun, Y. L. Xue, G. Y. Yao and S. L. Zheng, *Adv. Powder Technol.*, 2016, **27**, 330–337.
- 215 T. W. Wu, H. T. Zhao, X. J. Zhu, Z. Xing, Q. Liu, T. Liu, S. Y. Gao, S. Y. Lu, G. Chen, A. M. Asiri, Y. N. Zhang and X. P. Sun, *Adv. Mater.*, 2020, **32**, 2000299.
- 216 C. J. Shuai, B. Wang, S. Z. Bin, S. P. Peng and C. D. Gao, *ACS Appl. Mater. Interfaces*, 2020, **12**, 23464–23473.
- 217 S. Hejazi, S. Mohajernia, B. Osuagwu, G. Zoppellaro, P. Andryskova, O. Tomanec, S. Kment, R. Zbořil and P. Schmuki, *Adv. Mater.*, 2020, **32**, 1908505.
- 218 L. X. Zheng, F. Teng, X. Y. Ye, H. J. Zheng and X. S. Fang, *Adv. Energy Mater.*, 2020, **10**, 1902355.
- 219 M. Xiao, L. Zhang, B. Luo, M. Q. Lyu, Z. L. Wang, H. M. Huang, S. C. Wang, A. J. Du and L. Z. Wang, *Angew. Chem., Int. Ed.*, 2020, **132**, 7297–7301.
- 220 C. Q. Li, Z. M. Sun, W. Z. Zhang, C. H. Yu and S. L. Zheng, *Appl. Catal., B*, 2017, **220**, 272–282.
- 221 L. T. Ma, H. Q. Fan, K. Fu and Y. W. Zhao, *ChemistrySelect*, 2016, **1**, 3730–3738.
- 222 D. H. Xia, W. J. Wang, R. Yin, Z. F. Jiang, T. C. An, G. Y. Li, H. J. Zhao and P. K. Wong, *Appl. Catal., B*, 2017, **214**, 23–33.
- 223 Z. Y. Zhu, F. Zhou and S. Zhan, *Appl. Surf. Sci.*, 2019, **506**, 144934.
- 224 W. L. Shi, C. Liu, M. Y. Li, X. Lin, F. Guo and J. Y. Shi, *J. Hazard. Mater.*, 2020, **389**, 121907.
- 225 X. K. Zeng, S. Y. Lan and I. M. C. Lo, *Environ. Sci.: Nano*, 2019, **6**, 610–623.
- 226 S. L. Ma, S. H. Zhan, Y. G. Xia, P. F. Wang, Q. L. Hou and Q. X. Zhou, *Catal. Today*, 2019, **330**, 179–188.
- 227 Y. Huo, Z. L. Wang, J. F. Zhang, C. H. Liang and K. Dai, *Appl. Surf. Sci.*, 2018, **459**, 271–280.
- 228 M. Mitsushio, K. Miyashita and M. Higo, *Sens. Actuators, A*, 2006, **125**, 296–303.
- 229 Z. J. Zhang, W. Z. Wang, E. Gao, S. M. Sun and L. Zhang, *J. Phys. Chem. C*, 2012, **116**, 25898–25903.
- 230 F. F. Mei, K. Dai, J. F. Zhang, W. Y. Li and C. H. Liang, *Appl. Surf. Sci.*, 2019, **488**, 151–160.
- 231 K. H. Leong, B. L. Gan, S. Ibrahim and P. Saravanan, *Appl. Surf. Sci.*, 2014, **319**, 128–135.
- 232 Z. Y. Zhang, C. L. Shao, X. H. Li, C. H. Wang, M. Y. Zhang and Y. C. Liu, *ACS Appl. Mater. Interfaces*, 2010, **2**, 2915–2923.
- 233 J. Hu, Z. X. Zhong, F. Zhang, W. H. Xing, W. Q. Jin and N. P. Xu, *Ind. Eng. Chem. Res.*, 2016, **55**, 6661–6670.
- 234 Y. H. Ao, K. D. Wang, P. F. Wang, C. Wang and J. Hou, *Appl. Catal., B*, 2016, **194**, 157–168.
- 235 T. S. Sreena, P. P. Rao, A. K. V. Raj and T. R. A. Thara, *J. Alloys Compd.*, 2018, **751**, 148–158.
- 236 F. Schuster, B. Laumer, R. R. Zamani, C. Magén, J. R. Morante, J. Arbiol and M. Stutzmann, *ACS Nano*, 2014, **8**, 4376–4384.
- 237 W. L. Shi, M. Y. Li, X. L. Huang, H. J. Ren, F. Guo, Y. B. Tang and C. Y. Lu, *Chem. Eng. J.*, 2020, **394**, 125009.
- 238 H. Y. Xing, L. E. Z. G. Guo, D. Zhao and Z. F. Liu, *Chem. Eng. J.*, 2020, **394**, 124907.
- 239 Z. L. Jin, X. Yan and X. Q. Hao, *J. Colloid Interface Sci.*, 2020, **569**, 34–49.
- 240 Z. Z. Ai, K. Zhang, B. Chang, Y. L. Shao, L. Zhang, Y. Z. Wu and X. P. Hao, *Chem. Eng. J.*, 2020, **383**, 123130.
- 241 A. H. Yangjeh, M. Pirhashemi and S. Ghosh, *J. Alloys Compd.*, 2020, **826**, 154229.





- 242 C. H. Shen, X. J. Wen, Z. H. Fei, Z. T. Liu and Q. M. Mu, *Chem. Eng. J.*, 2020, **391**, 123612.
- 243 H. X. Shi, J. Fan, Y. Y. Zhao, X. Y. Hu, X. Zhang and Z. S. Tang, *J. Hazard. Mater.*, 2020, **381**, 121006.
- 244 C. J. Zhang, W. H. Fei, H. Q. Wang, N. J. Li, D. Y. Chen, Q. F. Xu, H. Li, J. H. He and J. M. Lu, *J. Hazard. Mater.*, 2020, **399**, 123109.
- 245 J. L. Zhou, Z. Q. Zhang, X. L. Kong, F. He, R. X. Zhao, R. Z. Wu, T. Wei, L. Wang and J. Feng, *Appl. Surf. Sci.*, 2020, **510**, 145442.
- 246 D. L. Han, Y. J. Han, J. Li, X. M. Liu, K. W. K. Yeung, Y. F. Zheng, Z. D. Cui, X. J. Yang, Y. Q. Liang, Z. Y. Li, S. L. Zhu, X. B. Yuan, X. B. Feng, C. Yang and S. L. Wu, *Appl. Catal., B*, 2020, **261**, 118248.
- 247 J. L. Huang, J. F. Zhou, J. Y. Zhuang, H. Z. Gao, D. H. Huang, L. X. Wang, W. L. Wu, Q. B. Li, D. P. Yang and M. Y. Han, *ACS Appl. Mater. Interfaces*, 2017, **9**, 36606–36614.
- 248 P. L. Yu, Y. J. Han, D. L. Han, X. M. Liu, Y. Q. Liang, Z. Y. Li, S. L. Zhu and S. L. Wu, *J. Hazard. Mater.*, 2020, **390**, 122126.
- 249 Y. P. Wang, F. C. Jiang, J. F. Chen, X. F. Sun, T. Xiao and H. Yang, *Nanomaterials*, 2020, **10**, 178.
- 250 H. Y. Ding, D. L. Han, Y. J. Han, Y. Q. Liang, X. M. Liu, Z. Y. Li, S. L. Zhu and S. L. Wu, *J. Hazard. Mater.*, 2020, **393**, 122423.
- 251 R. Wang, X. Y. Kong, W. T. Zhang, W. X. Zhu, L. J. Huang, J. Wang, X. Zhang, X. N. Liu, N. Hu, Y. R. Suo and J. L. Wang, *Appl. Catal., B*, 2018, **225**, 228–237.
- 252 Y. X. Chen, P. L. Wang, Y. Liang, M. J. Zhao, Y. Y. Jiang, G. T. Guang, P. Zou, J. Zeng, Y. S. Zhang and Y. Wang, *J. Colloid Interface Sci.*, 2018, **536**, 389–398.
- 253 Y. C. Yan, X. Q. Zhou, P. Yu, Z. F. Li and T. L. Zheng, *Appl. Catal., A*, 2020, **590**, 117282.
- 254 L. Ghalamchi, S. Aber, V. Vatanpour and M. Kian, *J. Ind. Eng. Chem.*, 2019, **70**, 412–426.
- 255 W. J. Wang, T. C. An, G. Y. Li, D. H. Xia, H. J. Zhao, J. C. Yu and P. K. Wong, *Appl. Catal., B*, 2017, **217**, 570–580.
- 256 S. Vignesh, S. Suganthib, J. K. Sundar and V. Raj, *J. Ind. Eng. Chem.*, 2019, **76**, 318–332.
- 257 S. P. Adhikari, H. R. Pant, J. H. Kim, H. J. Kim, C. H. Park and C. S. Kim, *Colloids Surf., A*, 2015, **482**, 477–484.
- 258 B. K. Liu, L. L. Mu, X. L. Han, J. T. Zhang and H. Z. Shi, *J. Photochem. Photobiol., A*, 2019, **380**, 111866.
- 259 V. Shanmugam, A. L. Muppudathi, S. Jayavel and K. S. Jayapeiumal, *Arabian J. Chem.*, 2018, **3**, 2439–2455.
- 260 S. Vignesh, S. Suganthi, J. K. Sundar and V. Raj, *Appl. Surf. Sci.*, 2019, **488**, 763–777.
- 261 Y. P. Li, Q. Wang, L. Y. Huang, X. Q. Xu, M. Xie, H. Wang, S. Q. Huang, F. Zhang, Z. Y. Zhao and J. Yang, *J. Mater. Sci.: Mater. Electron.*, 2018, **30**, 2783–2794.
- 262 B. K. Liu, Y. J. Wu, J. T. Zhang, X. L. Han and H. Z. Shi, *J. Photochem. Photobiol., A*, 2019, **378**, 1–8.
- 263 I. Meenakshisundarama, S. Kalimuthua, G. Priya and S. Karthikeyan, *Mater. Res. Bull.*, 2019, **112**, 331–335.
- 264 S. Ghafoor, A. Inayat, F. Aftab, H. Duran, K. Kirchhoff, S. Waseem and S. N. Arshad, *J. Environ. Chem. Eng.*, 2019, **7**, 103452.
- 265 D. Sun, Y. Zhang, Y. F. Liu, Z. G. Wang, X. C. Chen, Z. Y. Meng, S. F. Kang, Y. Y. Zheng, L. F. Cui, M. L. Chen, M. D. Dong and B. Hu, *Chem. Eng. J.*, 2020, **384**, 123259.
- 266 C. L. Ai, S. C. Wu, L. Y. Li, Y. J. Lei and X. W. Shao, *Colloids Surf., A*, 2019, **583**, 123981.
- 267 H. X. Zhao, S. Chen, X. Quan, H. T. Yu and H. M. Zhao, *Appl. Catal., B*, 2016, **194**, 134–140.
- 268 M. A. Khan, S. Mutahir, F. Y. Wang, J. W. Zhou, W. Lei and M. Z. Xia, *Sol. Energy*, 2019, **186**, 204–214.
- 269 J. Deng, J. L. Liang, M. Li and M. P. Tong, *Colloids Surf., B*, 2017, **152**, 49–57.
- 270 S. Vignesh, M. A. Lakshmi and J. K. Sundar, *J. Mater. Sci.*, 2018, **29**, 10784–10801.
- 271 S. W. Zhao, M. Zheng, H. L. Sun, S. J. Li, Q. J. Pan and Y. R. Guo, *Dalton Trans.*, 2020, **49**, 3723–3734.
- 272 D. Ayodhya and G. Veerabhadram, *Mater. Res. Innovations*, 2020, **24**, 210–228.
- 273 C. Liu, Y. B. Tang, P. W. Huo and F. Y. Chen, *Mater. Lett.*, 2019, **257**, 126708.
- 274 H. Yan, Z. W. Zhu, Y. M. Long and W. F. Li, *J. Photochem. Photobiol., A*, 2020, **390**, 112297.
- 275 W. N. Shen, X. Wang, Y. F. Ge, H. Feng and L. J. Feng, *Colloids Surf., A*, 2019, **575**, 102–110.
- 276 D. Vidyasagar, A. Kulkarni, S. G. Ghugal and S. S. Umare, *J. Chem. Technol. Biotechnol.*, 2019, **94**, 761–767.
- 277 S. J. Gu, D. Zhang, S. R. Luo and H. Yang, *Int. J. Photoenergy*, 2019, **2019**, 1–9.
- 278 R. Gupta, B. Boruah, J. M. Modak and G. Madras, *J. Photochem. Photobiol., A*, 2019, **372**, 108–121.
- 279 R. Nithya and S. Ayyappan, *J. Photochem. Photobiol., A*, 2020, **398**, 112591.
- 280 M. A. Qamar, S. Shahid, M. Javed, S. Iqbal, M. Sher and M. B. Akbar, *J. Photochem. Photobiol., A*, 2020, **401**, 112776.
- 281 X. L. Geng, L. Wang, L. Zhang, H. Wang, Y. Y. Peng and Z. Y. Bian, *Chem. Eng. J.*, 2021, **420**, 129722.
- 282 D. Yan, X. Wu, J. Y. Pei, C. C. Wu, X. M. Wang and H. Y. Zhao, *Ceram. Int.*, 2020, **46**, 696–702.
- 283 A. Balapure, Y. Nikhariya, N. S. S. Boppudi, R. Ganesan and J. R. Dutta, *ACS Appl. Mater. Interfaces*, 2020, **12**, 21481–21493.
- 284 M. Faraji, N. Mohaghegh and A. Abedin, *J. Photochem. Photobiol. B*, 2018, **178**, 124–132.
- 285 Y. W. Sun, X. Qi, R. Q. Li, Y. T. Xie, Q. Tang and B. X. Ren, *Opt. Mater.*, 2020, **108**, 110170.
- 286 D. Sun, J. Mao, L. Cheng, X. L. Yang, H. Li, L. X. Zhang, W. Zhang, Q. Zhang and P. W. Li, *Chem. Eng. J.*, 2021, **418**, 129417.
- 287 L. W. Wang, X. Zhang, X. Yu, F. Gao, Z. Y. Shen, X. L. Zhang, S. G. Ge, J. Liu, Z. J. Gu and C. Y. Chen, *Adv. Mater.*, 2019, **31**, 1901965.
- 288 L. Du, C. Jin, Y. F. Cheng, L. Q. Xu, X. L. An, W. Shang, Y. P. Zhang and X. Rao, *J. Alloys Compd.*, 2020, **842**, 155612.
- 289 M. A. Qamar, S. Shahid, M. Javed, M. Sher, S. Iqbal, A. Bahadur and D. X. Li, *Colloids Surf., A*, 2021, **611**, 125863.
- 290 S. A. Younis, P. Serp and H. N. Nassar, *J. Hazard. Mater.*, 2021, **410**, 124562.



- 291 M. Sher, S. A. Khan, S. Shahid, M. Javed, M. A. Qamar, A. Chinnathambi and H. S. Almoallim, *J. Environ. Chem. Eng.*, 2021, **9**, 105366.
- 292 J. H. Thurston, A. J. Clifford, B. S. Henderson, T. R. Smith, D. Quintana, K. F. Cudworth, T. J. Lujan and K. A. Cornell, *ACS Appl. Bio Mater.*, 2020, **3**, 1681–1689.
- 293 M. Oves, M. O. Ansari, R. Darwesh, A. Hussian, M. F. Alajmi and H. A. Qari, *Coatings*, 2020, **10**, 950.
- 294 A. Ahmed, M. B. K. Niazi, Z. Jahan, T. Ahmad, A. Hussain, E. Pervaiz, H. A. Janjua and Z. Hussain, *Eur. Polym. J.*, 2020, **130**, 109650.
- 295 M. A. Qamar, S. Shahid and M. Javed, *Ceram. Int.*, 2020, **46**, 22171–22180.
- 296 C. Zhang, Y. Li, C. Wang and X. Y. Zheng, *Sci. Total Environ.*, 2021, **755**, 142588.
- 297 D. Ayodhya and G. Veerabhadram, *J. Mol. Struct.*, 2019, **1186**, 423–433.
- 298 S. P. Adhikari, G. P. Awasthi, J. Lee, C. H. Park and C. S. Kim, *RSC Adv.*, 2016, **6**, 55079–55091.
- 299 J. G. Du, Z. Xu, H. Li, H. J. Yang, S. J. Xu, J. Wang, Y. A. Jia, S. L. Ma and S. H. Zhan, *Appl. Surf. Sci.*, 2021, **541**, 148487.
- 300 G. D. Fan, B. H. Du, J. J. Zhou, W. W. Yu, Z. Y. Chen and S. W. Yang, *Appl. Catal., B*, 2020, **265**, 118610.
- 301 G. Y. Li, X. Nie, J. Y. Chen, Q. Jiang, T. C. An, P. K. Wong, H. M. Zhang, H. J. Zhao and H. Yamashita, *Water Res.*, 2015, **86**, 17–24.
- 302 G. D. Fan, B. H. Du, J. J. Zhou, Z. S. Yan, Y. F. You and J. Luo, *Chem. Eng. J.*, 2021, **404**, 126509.
- 303 W. N. Shen, X. Wang, Y. F. Ge, H. Feng and L. J. Feng, *Colloids Surf., A*, 2019, **575**, 102–110.
- 304 R. Cheng, L. J. Shen, J. H. Yu, S. Y. Xiang and X. Zheng, *Catalysts*, 2018, **8**, 406.
- 305 S. H. Zhan, Q. L. Hou, Y. Li, S. L. Ma, P. F. Wang, Y. A. Li and H. T. Wang, *RSC Adv.*, 2018, **8**, 34428–34436.
- 306 Y. Liu, X. K. Zeng, X. Y. Hu, J. Hu, Z. Y. Wang, Y. C. Yin, C. H. Sun and X. W. Zhang, *Catal. Today*, 2019, **335**, 243–251.
- 307 J. Xu, Q. Z. Gao, Z. P. Wang and Y. F. Zhu, *Appl. Catal., B*, 2021, **291**, 120059.
- 308 R. A. Rather and I. M. C. Lo, *Water Res.*, 2020, **168**, 115166.
- 309 M. Sher, M. Javed, S. Shahid, S. Iqbal, M. A. Qamar, A. Bahadur and M. A. Qayyum, *RSC Adv.*, 2021, **11**, 2025–2039.
- 310 W. J. Wang, J. C. Yu, D. H. Xia, P. K. Wong and Y. C. Li, *Environ. Sci. Technol.*, 2013, **47**, 8724–8732.

